A Cholesterol-Based Allostery Model of T Cell Receptor Phosphorylation

Swamy, Mahima; Beck-Garcia, Katharina; Beck-Garcia, Esmeralda; Hartl, Frederike A.; Morath, Anna; Yousefi, O. Sascha

Published in:
Immunity

DOI:
10.1016/j.immuni.2016.04.011

Publication date:
2016

Document Version
Peer reviewed version

Research Article

A cholesterol-based allostery model of T cell receptor phosphorylation

Mahima Swamy[1,2,8], Katharina Beck-Garcia[1,3,8], Esmeralda Beck-Garcia[1,4], Frederike A. Hartl[1], Anna Morath[1,3], O. Sascha Yousefi[1,3], Elaine Pashupati Dopfer[1], Eszter Molnár[1], Anna K. Schulze[5,6], Raquel Blanco[7], Aldo Borroto[7], Nadia Martín-Blanco[7], Balbino Alarcon[7], Thomas Höfer[5,6], Susana Minguet[1,9] and Wolfgang W. A. Schamel[1,9]

[1]Department of Immunology, BIOSS Centre for Biological Signalling Studies, Faculty of Biology, and Centre for Chronic Immunodeficiency CCI, University Clinics Freiburg and Medical Faculty, Albert-Ludwigs-University of Freiburg, and Max Planck-Institute of Immunobiology and Epigenetics, 79104 Freiburg, Germany

[2]Division of Cell Signalling and Immunology, College of Life Sciences, University of Dundee, DD3 6PW, United Kingdom

[3]Spemann Graduate School of Biology and Medicine (SGBM), Albert-Ludwigs-University Freiburg, 79104 Freiburg, Germany

[4]International Max Planck-Research School for Molecular and Cellular Biology (IMPRS-MCB).

[5]Division of Theoretical Systems Biology, German Cancer Research Center (DKFZ), 69120 Heidelberg, Germany

[6]BioQuant Center, University of Heidelberg, 69120 Heidelberg, Germany

[7]Centro de Biología Molecular Severo Ochoa, CSIC-UAM, 28049 Madrid, Spain

[8]Co-first author

[9]Co-senior author

Contact: E-mail: wolfgang.schamel@biologie.uni-freiburg.de

SUMMARY

Signaling through the T cell receptor (TCR) controls adaptive immune responses. Antigen binding to the TCRαβ subunits transmits signals through the plasma membrane to induce phosphorylation of the CD3 cytoplasmic tails by incompletely understood mechanisms. Here we show that cholesterol bound to the TCRβ transmembrane region keeps the resting TCR in an inactive conformation that cannot be phosphorylated by active kinases. Only TCRs that spontaneously detach from cholesterol can switch to the active conformation and be phosphorylated. Indeed, by modulating cholesterol binding genetically or enzymatically, we can switch the TCR between the inactive and active states. The active conformation is stabilized by binding to peptide-MHC ligands, which thus control TCR signaling. Collectively, these data are explained by a model of reciprocal allosteric regulation of TCR phosphorylation by cholesterol and ligand binding. Our results provide both a molecular mechanism and a conceptual framework for how lipid-receptor interactions regulate signal transduction.

INTRODUCTION

Membrane lipids are thought to play a passive role in the function of transmembrane (TM) proteins by embedding and organizing them into lipid microdomains (Coskun and Simons, 2011). However, in a few cases it was shown that the TM regions of proteins and certain lipids interact in a specific manner (Cherezov et al., 2007; Contreras et al., 2012; Coskun and Simons, 2011; Hanson et al., 2008). The functional implications of these interactions remain mostly unknown. We have previously found that the TCR specifically binds to cholesterol in resting cells to aid formation of TCR nanoclusters (Molnar et al., 2012). Here, we investigate whether this binding also regulates TCR signaling.

The TCR consists of eight TM proteins organized in dimers; TCRαβ, CD3εγ, CD3εδ, CD3ζζ. TCRαβ binds to peptides presented on major histocompatibility complex (pMHC) molecules (Davis et al., 1998). The information on pMHC binding is transferred to the CD3 subunits, which are subsequently phosphorylated on immunoreceptor tyrosine-based activation motifs (ITAMs) by the Src-family tyrosine kinase Lck (Iwashima et al., 1994). Phospho-CD3s serve as docking sites for the kinase ZAP70 that becomes active at the TCR and transmits downstream signals.

The mechanism of signal transduction from the extracellular domains of TCRαβ through the membrane, resulting in phosphorylation of the CD3 cytoplasmic tails, is poorly understood (Davis and van der Merwe, 2006). Any mechanistic model needs to take into account that in resting T cells a large proportion of Lck is active (Nika et al., 2010), yet CD3s are not phosphorylated. Accordingly, several models have been proposed, including spatial segregation of phosphatases or sequestration of the CD3 chains (James and Vale, 2012; Kuhns and Davis, 2012; Shi et al., 2013; van der Merwe and Dushek, 2011; Xu et al., 2008).

Using protease resistance, FRET and various biochemical approaches, it was shown that the quaternary structure of the TCR changes upon ligand binding, resulting in a reversible conformational change in the cytoplasmic tails of the CD3 subunits (Gil et al., 2002; Lee et

al., 2015; Risueno et al., 2005; Risueno et al., 2008). These studies led to the permissive geometry model of TCR activation (Minguet and Schamel, 2008; Minguet et al., 2007). One hallmark of this structural change is the regulation of the accessibility of a proline-rich sequence (PRS) in the CD3ε cytosolic tail. In the resting, non-ligand-bound TCR state, the PRS cannot bind to the SH3.1 domain of the adaptor protein Nck hereafter referred to as inactive TCR or TCR_I. By contrast, in the ligand-bound TCR state, the PRS can bind to SH3.1; the TCR in this state is called here the active TCR or TCR_A. The switch from TCR_I to TCR_A is required for T-cell activation. This has been demonstrated by synthetic ligands that only evoked CD3 phosphorylation when the TCR_A form was stabilized (Minguet et al., 2007) and by identifying point mutations in the extracellular stalk region of CD3ε (such as K76T and C80G) that prevented the TCR_I to switch to TCR_A and abrogated CD3 phosphorylation (Blanco et al., 2014; Martinez-Martin et al., 2009).

Here, we provide mechanistic and quantitative insight into how pMHC-binding results in the phosphorylation of the TCR. We present biochemical, genetic and functional evidence that cholesterol and pMHC/antibody ligands regulate the allosteric transitions of the TCR: in the resting state cholesterol binding stabilizes TCR_I, ligand binding stabilizes TCR_A, and only TCR_A can be phosphorylated.

RESULTS

Cholesterol binds to TCRβ only in the resting, inactive TCR

Within the TCR, cholesterol specifically binds to TCRβ (Molnar et al., 2012). We asked whether this binding changes upon switching the conformation from TCR_I to TCR_A in living cells. We grew Jurkat T cells in the presence of a radioactive cholesterol analogue with a UV-inducible cross-linker group (photocholesterol) (Thiele et al., 2000). The cells were left unstimulated or stimulated with anti-CD3ε antibodies for different times before exposure to

UV light (Figure 1A). Subsequently, surface TCRs were isolated to detect the radioactive cholesterol signals by SDS-PAGE and autoradiography (Figure 1B). Anti-CD3 Western blotting (WB) served as loading control. Binding of cholesterol to TCRβ was reduced by more than 50% upon antibody-binding to the TCR. Alternative experimental settings corroborated this finding (Figure S1A and S1B). In parallel, an SH3-pull-down (PD) assay using the SH3.1 domain of Nck (Gil et al., 2002) was done to quantify the amount of TCR_A (Figure 1C and S1C). The reduction of cholesterol binding occurred concomitantly with the switch to TCR_A and might have preceded phosphorylation of CD3ζ (Figure 1C). As a control, UV-irradiation alone had no effect on the TCR_I-TCR_A equilibrium (Figure S1D). Thus, in living cells cholesterol preferentially binds to TCR_I.

To determine whether the inability of TCR_A to bind cholesterol is an intrinsic property of the TCR, we used a recently developed cholesterol-PD assay (Beck-Garcia et al., 2013) (Figure 1D). Cholesterol binding was indeed reduced when TCR_A accumulated due to anti-CD3ε or anti-TCRβ binding and was independent of phosphorylation, since it also occurred at 0°C and in the presence of the Src kinase inhibitor PP2 (Figure 1E). Bub3, which also binds to the lipid beads (Beck-Garcia et al., 2013), served as a loading control. This reduction was also seen in primary human T cells (Figure S1E). In contrast to cholesterol beads, TCR binding to stearate or palmitate beads was independent of the TCR conformational state (Figure S1F, S1G, 1F and S1H). Thus, the conformational state of the TCR specifically correlated with cholesterol binding (Figure 1F).

To support the finding that cholesterol preferentially binds to TCR_I compared to TCR_A, we used a CD3ε with a mutation (K76T) in its extracellular stalk region, which favors the inactive conformation (Martinez-Martin et al., 2009) (Figure 1G). We expressed murine wild type (wt) and K76T CD3ε in Jurkat cells (Figure S1I). Consistent with its inability to switch to TCR_A, similar amounts of K76T TCR bound to cholesterol beads with or without antibody

stimulation (Figure 1H). Altogether, these data confirm that cholesterol binding to the TCR is conformation-selective.

Cholesterol binding keeps the TCR in the non-phosphorylatable state

To construct a TCRβ chain that cannot bind cholesterol, we took advantage of our finding that the γδ TCR does not bind cholesterol (Figure S2A). We surmised that cholesterol binds to the TCRβ TM region. Thus, a single-chain Fv fragment-tagged TCRβ chain (scTCRβ) (Gil et al., 2002) mutant was constructed, in which the TM region was replaced with the TM from the human TCRγ2 chain (TMchim, Figures 2A, S2B and S2C). The TMchim TCR was expressed on the surface of TCRβ-negative Jurkat cells to the same levels as the wt TCR (Figure S2D). Native gel and epitope accessibility analyses suggested that the TMchim TCR assembled in the same stoichiometry and a similar structure as the wt TCR (Figures S2E and S2F). However, the resting TMchim TCR bound more weakly to cholesterol compared to the resting wt TCRs (Figure 2B), indicating that indeed the TCRβ TM region binds cholesterol. The residual binding of the TMchim TCR to the cholesterol-beads was not further decreased by antibody-stimulation and had the same level as the cholesterol-binding of the antibody-stimulated wt TCR (Figure 2B). This suggested that the TMchim TCR does not bind to cholesterol. As a control, TMchim and wt TCRs bound equally well to palmitate-coupled beads (Figure S2G).

Importantly, reduced cholesterol binding to the TMchim TCR promoted the active conformation as seen by increased binding in the SH3-PD assay in both resting and anti-CD3ε-stimulated conditions (Figure 2C). The increased levels of TCR_A resulted in enhanced basal and antibody-induced phosphorylation of CD3 (Figure 2D). This increase in CD3 phosphorylation was physiologically relevant, since we also detected enhanced Erk phosphorylation and upregulation of the activation marker CD69 in the resting and in the

antibody-stimulated situation (Figure 2E and S2H). In conclusion, genetically ablating the cholesterol-binding region in the TCR increased the frequency of TCR_A indicating that cholesterol binding regulates the TCR_I-TCR_A equilibrium.

Cholesterol removal causes TCRs to switch to the active state

Next, we tested whether cholesterol stabilizes the inactive state in native, wt TCRs (Figure 3A). Reduction of cell membrane cholesterol levels by treatment with cholesterol oxidase, which converts cholesterol to cholest-4-en-3-one (Gimpl and Gehrig-Burger, 2007), led to a 2-fold increase in the proportion of TCR_A (Figure 3B). Moreover, lowering cholesterol levels enhanced basal CD3ζ and Erk phosphorylation (Figure 3B and 3C) as well as CD69 upregulation (Figure S3A) in Jurkat cells. Enhanced Erk phosphorylation upon cholesterol reduction was also seen in primary human T cells (Figure S3B). Cholesterol oxidase treatment neither led to decreased cell viability (Figure S3C) nor rendered the cells unresponsive to anti-CD3 stimuli (data not shown). Switching to TCR_A and increased CD3ζ phosphorylation were also seen after we extracted cholesterol using methyl-β-cyclodextrin (mβCD, Figure S3D).

The induction of signaling by cholesterol removal using mβCD is in line with the literature (Kabouridis et al., 2000; Rouquette-Jazdanian et al., 2006), and could be due to either the accumulation of TCR_A or to other effects of cholesterol reduction, such as altered membrane microdomain organization (Horejsi, 2003). To test whether the stimulating effect of cholesterol is TCR-dependent, we used TCR-negative Jurkat cells. Cholesterol oxidase treatment did not lead to increased Erk phosphorylation in cells lacking a TCR (Figure 3D). Hence, enhanced signaling upon cholesterol extraction was TCR-dependent, and thus most likely caused by the accumulation of TCR_A. Consistent with this conclusion, we found that in cells expressing the TMchim TCR, which does not bind cholesterol, cholesterol oxidation did not further increase the amount of TCR_A or Erk phosphorylation (Figure S3E). Together,

these data suggest that cholesterol-binding to the TCR keeps the TCR in the TCR_I state to prevent spontaneous signaling.

Cholesterol detachment and switching to TCR_A favor CD3 phosphorylation

To confirm a gatekeeper function of cholesterol, we investigated whether cholesterol removal from the TCR is required for CD3 phosphorylation. We grew Jurkat cells in radioactive photocholesterol as before. Using UV light, we covalently linked cholesterol to the TCRs, hypothesizing that cholesterol-linked TCRs would not be able to spontaneously switch to the TCR_A form, and therefore would not become phosphorylated. To detect CD3 phosphorylation, we used the phosphatase inhibitor pervanadate that prevents removal of phosphate groups from CD3, hence allowing phosphorylated TCRs to accumulate; of note, pervanadate does not itself affect the TCR's conformational state (Gil et al., 2002; O'Shea et al., 1992). First, we cross-linked radioactive cholesterol to the TCRs and then treated the cells with pervanadate (Figure 4A and 4B, lane 1). After lysis, phosphorylated proteins were purified. The autoradiography shows that cholesterol-linked TCRs were not phosphorylated (lane 1). Due to the low amount of radioactive cholesterol, most TCRs were bound to endogenous unmodified cholesterol (Figure 4A, lower panel), and those TCRs were phosphorylated as demonstrated by WB (Figure 4B, lane 1). This indicated that the cholesterol-linked TCRs were locked in a non-phosphorylatable state, and that cholesterol needs to dissociate from the TCR before the TCR can be phosphorylated.

In contrast, when the cells were first treated with pervanadate to phosphorylate the TCRs and then exposed to UV light (Figure 4A and 4B, lane 2), radioactive and phosphorylated TCRs were detected. This served as a control for cross-linking of radioactive cholesterol to TCRβ and indicated that phosphorylated TCRs can switch to the TCR_I state and then bind to cholesterol again. Indeed, phosphorylated TCRs could switch back to TCR_I (Figure 4C, SH3-PD), and bind to cholesterol-coupled beads (Figure 4C, cholesterol-PD). UV light

illumination alone did not alter the phosphorylation of the TCR (Figure S4A). In conclusion, cholesterol-bound TCRs cannot be phosphorylated in living cells, confirming that only those TCRs that are not bound to cholesterol are capable of switching to TCR_A in order to be phosphorylated.

TCRs can spontaneously switch to TCR_A (de la Cruz et al., 2011; Mingueneau et al., 2008) and Figure 4B suggests that only TCR_A can be phosphorylated (Figure 4D, upper panel). To test if the switch to TCR_A is required for phosphorylation, we used the K76T CD3ε mutant, whose capacity to switch to the TCR_A conformation is reduced (Martinez-Martin et al., 2009) (Figure 4D, lower panel). The murine wt and K76T CD3ε-expressing Jurkat cells were treated with pervanadate, lysed, and the TCR was immuno-precipitated (Figure 4E). We used twice the amount of K76T CD3ε-expressing cells for the IP to compensate for the two-fold lower TCR expression level (Figure S1I). Indeed, similar amounts of TCRs were separated by SDS-PAGE (Figure 4E, lowest panel), but a smaller fraction of CD3ζ and CD3ε were phosphorylated in the K76T mutant (only TCR_I) compared to the wt TCR (spontaneously switching to TCR_A). Likewise, ZAP70 was more readily recruited to, and phosphorylated at, the wt TCR (Figure 4E and S4B). In addition, the upregulation of CD69 was impaired when the K76T CD3ε-containing TCR was stimulated with anti-CD3 compared to the wt TCR (Figure S4C).

Further, to compare cells with equal surface TCR expression levels, we used flow cytometry. We stimulated wt and K76T CD3ε-expressing Jurkat cells with pervanadate and stained them for flow cytometry against mouse CD3ε, phospho-ZAP70 and phospho-Erk. Cells expressing equal levels of mouse CD3 were gated. Again the downstream signaling events, such as phosphorylation of ZAP70 and Erk, were reduced when the K76T CD3ε-containing TCR was stimulated (Figure S4D, S4E and S4F).

We thus conclude that CD3 phosphorylation by a ligand-independent stimulus requires that the TCR spontaneously adopt the active conformation.

Lck can only phosphorylate TCR_A

To characterize the mechanism that allows TCR_A, but not TCR_I, to be phosphorylated, we used a synthetic system in which the wt scTCR (Gil et al., 2002) was purified using nitro-phenol-coupled beads without altering the TCR's conformational state. We then left the sample untreated (Figure 5A, TCR_I) or added anti-CD3 and anti-TCRβ antibodies that mimic ligand binding and stabilize TCR_A (Minguet et al., 2007). The system was supplemented with recombinant active Lck performing the *in vitro* kinase assay with the TCRs immobilized on the beads. In the untreated sample hardly any CD3ζ phosphorylation was detected (Figure 5B), suggesting that the CD3 tails were protected in the TCR_I conformation. Strikingly, CD3ζ, CD3ε and CD3δ (Figure 5B, 5C and S5A) were more strongly phosphorylated when TCR_A was stabilized by antibody binding. Further, the amount of TCR_A (Figure 5B, lower panel) correlated with the amount of TCRs that were phosphorylated (Figure 5B, upper panel) and with the intensity of downstream signaling (Figure S5B). Likewise, recombinant Lck could only phosphorylate membrane-embedded TCRs when anti-CD3ε antibodies (Figure 5D) or pMHC tetramers stabilized TCR_A (Figure S5C). Importantly, Lck autophosphorylation and LAT phosphorylation by Lck were detected independently of the TCR's conformational state, demonstrating that (i) Lck was active under all conditions and (ii) the TCR state specifically regulated the accessibility of the TCR cytoplasmic tails for phosphorylation (Figure 5B and 5D). Since the recombinant Lck did not contain any fatty acid modifications, differential TCR_A versus TCR_I phosphorylation cannot be caused by differential interaction of Lck with the detergent micelle. Addition of cholesterol to our synthetic reconstitution system reduced both the spontaneous and antibody-stabilized accessibility of the CD3ε's PRS

(TCR_A) and the amount of CD3 phosphorylation (Figure 5E, F). In conclusion, an active kinase can phosphorylate CD3 only when the TCR is in the active state.

An allostery model for the regulation of TCR activity

Based on our understanding of the initial steps of TCR triggering, we propose a quantitative model that describes how cholesterol and pMHC control the conformational equilibrium between the TCR_I and TCR_A states (Figure 6A). This model provides a mechanistic basis for our experimental observations and is based on five premises: (1) The TCR is in conformational equilibrium with the equilibrium constant $L = [TCR_I]/[TCR_A]$. Thus, the TCR can switch spontaneously in the absence of ligand to the active state, as suggested experimentally (de la Cruz et al., 2011; Mingueneau et al., 2008) (Figures 2 and 3). (2) The conformational switch is reversible in that TCR_A can revert to TCR_I. This was shown earlier (Minguet et al., 2007). (3) Cholesterol binds to TCR_I, but not to TCR_A, with the affinity constant K_c, hence stabilizing TCR_I (Figure 1). This is consistent with our finding that the conformational equilibrium of a mutant TCR that cannot bind cholesterol is shifted towards TCR_A (Figure 2). (4) Only TCR_A can be phosphorylated, suggested by our results using the *in vitro* kinase assay (Figure 5) and our findings that switching to TCR_A through reduced cholesterol binding results in spontaneous signaling (Figure 2 and 3). (5) Binding of at least dimeric soluble pMHC stabilizes TCR_A, while monovalent soluble pMHC can bind to both TCR_A and TCR_I as suggested earlier (Minguet et al., 2007). According to previous findings, we consider a preformed nanocluster of two TCRs (Schamel et al., 2005) and assume that conformational transitions in a TCR cluster are concerted (Martinez-Martin et al., 2009). The affinity constants for monovalent and bivalent pMHC binding are denoted by K_a and K_b, respectively. Assuming nanoclustering of the TCRs is not necessary; the behavior of the model is similar when single TCRs are clustered by being bound bi- or multivalently to pMHC (Figure S7).

To estimate the parameters of the model from the experimental data, we calculated the frequencies of TCR_A and TCR_I and their ligand-bound states in equilibrium as a function of K_a, K_b, K_c, L, and the concentrations of membrane cholesterol and pMHC (Supplemental Experimental Procedures). Quantifying the fraction of active TMchim TCR in unstimulated cells, which cannot bind cholesterol, we find $L = 14$ (Figure S6A). Thus, even in the absence of cholesterol the TCR has a strong propensity to be in the inactive state (7% of TMchim TCR are spontaneously switched to TCR_A). Cholesterol binding further lowers the TCR_A fraction 4 fold (only 2% of wt TCR are spontaneously switched to TCR_A); this yields K_c x [cholesterol] = 1.0 (Figure S6A). Thus, cholesterol strongly augments the intrinsic propensity of the TCR to be inactive. With an approximate cholesterol concentration in the plasma membrane of 1 cholesterol molecule/nm^2 (Falck et al., 2004), we obtain $K_c = 10^6$ m^2/mol for the cholesterol-TCR_I affinity (Figure S6B). Having fixed the parameters that define the resting state of the TCR, we tested the ability of the model to describe TCR activation. Stimulation of wt T cells with anti-CD3 experimentally increased the fraction of TCR_A from 2% to 16% (Figure S6A). Fitting the model to these numbers predicted a TCR_A fraction of 43% for the non-cholesterol binding TMchim TCR after the same anti-CD3 stimulus. We experimentally confirmed this prediction (40 ± 4%, Figure 6B). Taken together, these data show that this allosteric model quantitatively describes the active-inactive conformational equilibrium of the TCR and its regulation by cholesterol (all model parameters are listed in Figure S6B).

An unexpected prediction of the model was that the TCR conformation controls the TCR's avidity for pMHC, because only TCR_A can bind pMHC bivalently (Figure 6A). To test this prediction, we used the OT-1 TCR, which binds to OVA-H2-L^d MHC tetramers. The mutant D227K-H2-L^d molecule does not bind to CD8 (Potter et al., 1989), allowing us to analyze the TCR-pMHC interaction only. In agreement with the model, the C80G mutant OT1 TCR, which cannot switch to TCR_A (Martinez-Martin et al., 2009), binds less OVA-D227K-H2-L^d

MHC tetramers than the wt OT1 TCR (Figure 6C; points) (Blanco et al., 2014). Fitting the model to these data (Figure 6C, lines), we estimate K_a = 0.1 μM^{-1} and K_b = 1755, thus indicating that pMHC binding by TCR_A is preferred. Similar results were obtained when the MHC-CD8 interaction was not prevented (Figure S6C). In summary, the model predicts, and the experimental data confirm, strong reduction of pMHC tetramer binding by a mutant TCR that cannot switch to TCR_A.

Collectively, these data define the parameters for the allostery model of TCR regulation. The predicted dose-responses to pMHC ligand concentrations show quantitative control by cholesterol of TCR_A levels (Figure 6D). Moreover, cholesterol, through controlling the active-inactive state equilibrium, influences pMHC binding (Figure 6E). In conclusion, cholesterol emerges as a negative allosteric regulator of TCR activity that guards both the resting state of the TCR and modulates TCR activation by ligand.

DISCUSSION

In recent years, specific interactions between TM regions of proteins and membrane lipids have been discovered (Cherezov et al., 2007; Contreras et al., 2012; Coskun et al., 2011; Hanson et al., 2008) but not much is known about their functions. Here, we demonstrate that cholesterol binding to the TM region of TCRβ controls T-cell activation by regulating an allosteric switch in the TCR that exposes the CD3ε PRS (active TCR or TCR_A) and permits the phosphorylation of the ITAM tyrosines. This is achieved by selective cholesterol binding to the inactive TCR conformation (TCR_I), which prevents spurious TCR activation and sets the activation threshold for pMHC ligands. Our findings thus show how a specific membrane lipid regulates receptor function.

Our data indicate that prior to stimulation, the TCR exists in equilibrium between the TCR_I and TCR_A state. This is in line with earlier reports showing that a fraction of the TCRs are

spontaneously in the TCR_A state in unstimulated cells (de la Cruz et al., 2011; Mingueneau et al., 2008). We found that on a resting, mature T cell, 98% of the TCRs are in the TCR_I state, preventing spontaneous, ligand-independent signaling in T cells. In addition, spontaneous signaling is further controlled by the constant removal of CD3 phosphorylations by phosphatases, such as CD45 and CD148 located in the vicinity of the resting TCR (Choudhuri et al., 2005; Davis and van der Merwe, 2006). Our data strongly support that cholesterol binding stabilizes the TCR_I state. Hence, a prediction of our allosteric model is that the TCR_I-TCR_A equilibrium should be shifted towards the signaling competent TCR_A by reducing cholesterol binding. Indeed, we have reduced cholesterol-binding genetically (by exchanging the TCRβ TM region) and enzymatically (by oxidizing or extracting cholesterol) and show that the proportion of TCR_A increased, which led to increased spontaneous TCR-dependent signaling. Enhanced signaling in primary T cells had previously been noted in a transgenic mouse model expressing a similar chimeric TCR in which the TCRβ TM region had been exchanged with the one of TCRγ (Petersen et al., 2004); our findings now provide the molecular explanation for this observation.

To prove that the capacity to be phosphorylated is dependent on the conformational state of the TCR, we used the phosphatase inhibitor pervanadate, which leads to accumulation of phosphate groups at CD3 (O'Shea et al., 1992) without manipulating the TCR_I-TCR_A equilibrium (Gil et al., 2002). Neither the K76T CD3ε-containing TCR, which cannot switch to TCR_A, nor covalently cholesterol-linked TCRs, which are locked in the TCR_I state, were efficiently phosphorylated upon pervanadate treatment. This indicated that CD3 phosphorylation by a ligand-independent stimulus requires that the TCR spontaneously adopts the TCR_A conformation to be phosphorylated.

Our results raise the question of how ligand binding removes cholesterol from TCR_I. Our quantitative allosteric model suggests that cholesterol spontaneously associates to and dissociates from the TCR_I, with 50% of the TCR_Is being cholesterol-bound. Only when a

TCR_I is not bound to cholesterol, it can spontaneously switch to TCR_A. Then the TCR_A state can be stabilized by pMHC binding and cholesterol rebinding to TCR_A is prevented. We have previously hypothesized that ligand binding induces the TCR to switch to the active state (Gil et al., 2002; Minguet et al., 2007; Risueno et al., 2005). However, our new data suggest that this switch occurs spontaneously and ligand binding stabilizes TCR_A. Monovalent pMHC binding might be enough to stabilize the TCR_A conformation, when pMHC is tethered to a surface. However, we have used soluble pMHC tetramers to quantify pMHC binding. For soluble ligands it was shown that minimally, a dimeric pMHC is required to stabilize TCR_A (Minguet and Schamel, 2008) and thus, foster downstream signaling (Boniface et al., 1998; Cochran et al., 2000; Krogsgaard et al., 2005). This might be true in the case that the TCR was a preformed nanocluster (Schamel et al., 2005) or that two TCR monomers were held together by bivalent pMHC binding. The change in the quaternary structure of the TCR might include reorientation of one CD3ζ in respect to the second CD3ζ (Lee et al., 2015) without structural changes within one TCRαβ heterodimer (Minguet and Schamel, 2008).

Using quantitative data on the TCR conformational switch and our understanding of the role of cholesterol in regulating the TCR_I-TCR_A equilibrium, we developed a data-based mathematical model of the allosteric regulation of TCR phosphorylatability. In absence of cholesterol, 7% of the TCRs are in the TCR_A state. However, cholesterol tightens this regulation and only 2% of the TCRs are in the TCR_A state. This 3.5-fold increase corresponds to the narrow range of 2-4-fold increases in ITAM phosphorylation or ZAP70 recruitment upon TCR activation (Deswal et al., 2011; Kim and White, 2006; Steinberg et al., 2004). This increase is physiologically significant, since it results in initiation of TCR signaling as seen by phospho-Erk and CD69 upregulation. As allosteric effects are reciprocal (Monod et al., 1965), our model made the remarkable prediction that the TCR_I-TCR_A equilibrium should also affect pMHC binding. While there is much experimental evidence for the reverse statement (pMHC binding shifts the conformational equilibrium), this was an unexpected prediction given that

'retrograde' effects of the TCR on ligand binding have not been considered. Our subsequent experimental data supported this prediction, showing that soluble pMHC tetramers bind with higher avidity to wt TCRs compared to those that are locked in the TCR_I state. Thus the allostery model of TCR regulation proposed here implies that the avidity of a given TCR for antigen is not a constant but can be regulated by the conformational state of the TCR.

Using CD3 mutants and modified ligands, it was shown that the TCR_A state, as measured by the exposure of the CD3ε PRS, was required for ligand-induced CD3 phosphorylation and T cell activation (Martinez-Martin et al., 2009; Minguet et al., 2007). Since only the exposed PRS binds to Nck, it was suggested that Nck plays a role in CD3 phosphorylation (Blanco et al., 2014; Borroto et al., 2013; Mingueneau et al., 2008). However, our data suggest an alternative mechanism. Only in the TCR_A state, and not in the TCR_I state, the ITAM tyrosines are phosphorylatable. This provides a molecular mechanism for how non-triggered TCRs are protected from phosphorylation in the presence of active Lck (Nika et al., 2010). Hence, our model explains how cholesterol aids to keep the TCR inactive and how ligand-binding induces TCR phosphorylation by stabilizing TCR_A. The molecular events described in our novel model most likely precede the phosphorylation- or Ca^{2+} influx-induced dissociation of the CD3ε and CD3ζ cytoplasmic tails from the plasma membrane (Aivazian and Stern, 2000; Shi et al., 2013; Xu et al., 2008).. In fact these mechanisms might serve to facilitate further phosphorylation and hence, sustain T-cell activation signals.

It has been reported that extraction of cholesterol using methyl-β-cyclodextrin (mβCD) followed by antibody stimulation leads to reduced TCR signaling, most likely due to disruption of lipid rafts (Montixi et al., 1998; Xavier et al., 1998). In contrast, when mβCD is used as a stimulus, i.e. when signaling is analyzed immediately after the mβCD treatment, the TCR is triggered (Kabouridis et al., 2000; Rouquette-Jazdanian et al., 2006). We now provide a molecular mechanism for the stimulatory effect of mβCD, by demonstrating that lowering

cholesterol levels leads to an increase in TCR_A that can be phosphorylated. Our data also suggest that cholesterol exerts its effect on TCR signaling directly at the TCR, since (i) cholesterol oxidation did not induce signaling in a TCR-deficient T cell line, (ii) the TMchim TCR showed enhanced signaling and (iii) binding of cholesterol to the TCR prevented CD3 phosphorylation.

Our new findings can be integrated with existing models of TCR activation and several molecular events might occur simultaneously. The change in the conformational state of the TCR most likely includes the TM regions, such as the one of TCRβ (this study) and CD3ζ (Lee et al., 2015), the cytoplasmic tails of CD3ε, CD3γ, CD3δ and CD3ζ (Gil et al., 2002; Risueno et al., 2008; Xu et al., 2008)(this study) and the extracellular arrangement of at least two TCRs (this study). At the same time ligand binding could segregate phosphatases from the TCR to allow phosphorylation to accumulate (Choudhuri et al., 2005; Davis and van der Merwe, 2006). Aggregation of TCRs could increase the local concentration of Lck and reduce the lateral mobility of the receptor, co-clustering of the TCR with the co-receptors CD4 and CD8 might stabilize the pMHC TCR interaction and recruit additional Lck molecules. Further, mechanical forces elicited by pMHC binding (Kim et al., 2009) as well as other lipids might play a role.

Cholesterol is also involved in the formation of TCR nanoclusters (Molnar et al., 2012; Schamel et al., 2005), and thus has two apparently opposing effects in respect to pMHC binding. By inducing TCR nanoclustering, cholesterol enhances the avidity towards pMHC tetramers. In contrast, by stabilizing the TCR_I state, cholesterol decreases the avidity. Using our mathematical model, we simulated reduction of the cholesterol concentration and found that the impact of changing the TCR_I-TCR_A equilibrium on pMHC tetramer binding is rather small (maximal 3 fold). Furthermore, experimental cholesterol-extraction reduced pMHC tetramer-binding to T cells (Fahmy et al., 2001; Molnar et al., 2012). Thus, the nanoclustering function of cholesterol predominates in regulating the avidity towards pMHC tetramers. We

suggest that cholesterol has a dual role at the TCR, enhancing the sensitivity to agonistic ligands but still restraining spontaneous signaling, which might be especially important in the case of antigen-experienced T cells (Kumar et al., 2011). Since different T cell developmental and differentiation stages contain different levels of cholesterol (Brumeanu et al., 2007; Kaech et al., 2002; Tani-ichi et al., 2005), it could be that changes in the plasma membrane cholesterol level contribute to regulate TCR activity and thereby, T cell sensitivity *in vivo*.

In conclusion, we show here that the specific interaction of the TCRβ TM region with cholesterol regulates TCR triggering and T cell activation. In contrast to the long-standing assumption that the plasma membrane is an inert solvent that does not impact on the conformation or activity of membrane proteins, we clearly demonstrate that cholesterol binding to the TCR regulates CD3 phosphorylability. Lipids therefore not only play a role in the activation of T cells but also in guarding their resting state. Our work provides a novel paradigm for how the activity of TM proteins can be regulated.

EXPERIMENTAL PROCEDURES

Photocholesterol labelling

[3α-^{3}H]6-azi-5α-cholestan-3α-ol (radioactive UV-light cross-linkable cholesterol, photocholesterol) was provided by Dr. Thiele. Jurkat cells were incubated for 16 hours in lipid-free medium containing a radioactive cross-linkable cholesterol-mβCD complex (5 μCi/ml) and UV-irradiated for 30 seconds, before or after the indicated times of adding the stimulus (anti-CD3, UCHT1, or anti-TCRβ, Jovi1). After cell lysis, IPs were performed as indicated. Samples were separated by running two SDS-PAGE gels in parallel. One gel was dried and exposed to an X-ray film (autoradiography), and the corresponding second gel subjected to WB. Alternatively, membrane patches were prepared as outlined above, the

TCR_A state-stabilizing antibody was given at 37°C and after UV irradiation, the membranes were lysed and analysed as above.

Synthesis of beads coupled to stearate, palmitate and cholesterol

The synthesis of the stearate-, palmitate- and cholesterol-coupled sepharose beads was as described (Beck-Garcia et al., 2013). In brief, the carboxygroups of stearate, palmitate or cholesteryl hemisuccinate were activated by N,Ndiisopropyl-ethylamine and O-(benzotriazol-1-yl)-tetramethyluronium tetrafluoroborate and coupled to ω-aminohexyl agarose beads. The completeness of the reaction was tested by a Kaisertest.

SH3-PD assay, lipid-PD assay, IP and immunoblotting

Lysates were subjected to the SH3-PD assay using SH3.1(Nck)-GST bound glutathione-coupled beads as described (Gil et al., 2002). The cholesterol-, stearate- and palmitate-PD assays were also done as described (Beck-Garcia et al., 2013); after the PD the beads were washed 3 times with lysis buffer containing 0.05-0.5% Brij96V. In these PD assays, the detergent molecules and possibly some of the endogenous lipids, are bound to the TM regions of the TCR. Thus, those molecules might have mediated or modified the interaction of the lipid-coupled beads with the TCR. However, radioactive cholesterol was directly crosslinked to the TCRβ chain, showing that cholesterol directly binds to the TCR in living cells.

Anti-TCR IPs were performed with 2 μg of anti-CD3ε or anti-TCRβ antibodies overnight at 4°C. Anti-phosphotyrosine IPs were performed with anti-phospho-tyrosine antibody (PT-66)-coupled beads (Sigma). Samples were subjected to SDS-PAGE separation and transferred to PVDF membranes. Western blotting (WB) was performed by conventional methods. Quantifications of the band intensities were done with the Image Studio Ver 2.0 (LI-COR), with the ImageJ program or the ImageQuantTL software (GE Healthcare) after fluorescence or chemoluminescence detection.

Reconstitution of CD3 phosphorylation

2 x 10^8 31-13.scTCRβ cells were lysed in lysis-buffer containing 1% digitonin or 0.5% Brij96V. The lysate was divided into equal parts. One part of the lysate was left untreated, and 5 μg of anti-CD3ε antibody (OKT3 or UCHT1) or anti-TCRβ antibody (Jovi1) was added to the other parts. Antibodies were allowed to bind to the scTCR on ice for 30-90 min. 7 mM cholesterol in EtOH or EtOH alone was then added when indicated. Afterwards, the scTCRs (and bound antibodies) were purified with nitro-phenol-coupled-sepharose beads. After washing, 50 ng active, recombinant GST-Lck and 1 μM ATP were added in kinase-buffer (40 mM HEPES, 10 mM $MgCl_2$, 2 mM $MnCl_2$) and incubated for the indicated times at 37°C. Presence of the TCR_A state or antibody binding to the TCR was controlled by SH3-PD or binding to protein G-sepharose, respectively.

Upregulation of CD69

To quantify the degree of T-cell activation, we stimulated the cells for 6-7 hours with the indicated stimuli. After harvesting, cells were stained with an APC-coupled anti-CD69 antibody (Invitrogen), washed and analyzed with a Calibur (BD Biosciences) or a Gallios (Beckman Coulter) flow cytometer. Fluorescence intensities were analyzed with FlowJo 8.2 software.

Statistical analysis

Error bars depict standard error of the mean (SEM). Statistical significance and linear regression were determined with GraphPad Prism as indicated: * $p < 0.05$, ** $p < 0.01$, *** $p < 0.001$. The significances were calculated by Student´s t-test as indicated (see below).

Supplemental Information

Supplemental Information includes six figures and Supplemental Experimental Procedures.

Author Contributions MS, KBG, EBG, EPD, FAH, OSY, AM, EM, RB, NMB and SM designed and performed experiments. TH and AS designed and conducted the mathematical modelling. AB and BA contributed with reagents. SM and WWS conceived and coordinated the project and designed the experiments. WWS, SM, MS and TH wrote the manuscript. All authors discussed the results and provided intellectual input at all stages.

Acknowledgements We thank Kerstin Fehrenbach for technical assistance, Pete Nielsen for reading the manuscript, Immanuel Lüscher, Ed Palmer and Christoph Thiele for providing reagents and Uenal Coskun and Aleksander Czogalla for discussions. This work was funded by the EU through grant FP7/2007-2013 (SYBILLA, BA, TH, WWS) and ERC 2013-Advanced Grant 334763 (NOVARIPP, BA) and the Deutsche Forschungsgemeinschaft (DFG) through EXC294 (the Center for Biological Signalling Studies, *BIOSS*, WWS), EXC81 (CellNetworks, TH), GSC-4 (Spemann Graduate School, KBG, OSY, AM) and grant SCHA 976/2-1 (WWS).

REFERENCES

Aivazian, D., and Stern, L.J. (2000). Phosphorylation of T cell receptor zeta is regulated by a lipid dependent folding transition. Nat. Struct. Biol. 7, 1023-1026.

Beck-Garcia, E., Beck-Garcia, K., Schlosser, A., and Schamel, W.W. (2013). Analysis of interactions between proteins and fatty acids or cholesterol using a fatty acid/cholesterol pull-down-assay. Anal. Biochem. 436, 75-77.

Blanco, R., Borroto, A., Schamel, W., Pereira, P., and Alarcon, B. (2014). Conformational changes in the T cell receptor differentially determine T cell subset development in mice. Sci Signal 7, ra115.

Boniface, J.J., Rabinowitz, J.D., Wülfing, C., Hampl, J., Reich, Z., Altman, J.D., Kantor, R.M., Beeson, C., McConnell, H.M., and Davis, M.M. (1998). Initiation of signal transduction through the T cell receptor requires the peptide multivalent engagement of MHC ligands. Immunity 9, 459-466.

Borroto, A., Arellano, I., Dopfer, E.P., Prouza, M., Suchanek, M., Fuentes, M., Orfao, A., Schamel, W.W., and Alarcon, B. (2013). Nck Recruitment to the TCR Required for ZAP70 Activation during Thymic Development. J. Immunol. 190, 1103-1112.

Brumeanu, T.D., Preda-Pais, A., Stoica, C., Bona, C., and Casares, S. (2007). Differential partitioning and trafficking of GM gangliosides and cholesterol-rich lipid rafts in thymic and splenic CD4 T cells. Molec. Immunol. 44, 530-540.

Cherezov, V., Rosenbaum, D.M., Hanson, M.A., Rasmussen, S.G., Thian, F.S., Kobilka, T.S., Choi, H.J., Kuhn, P., Weis, W.I., Kobilka, B.K., and Stevens, R.C. (2007). High-resolution crystal structure of an engineered human beta2-adrenergic G protein-coupled receptor. Science 318, 1258-1265.

Choudhuri, K., Wiseman, D., Brown, M.H., Gould, K., and van der Merwe, P.A. (2005). T-cell receptor triggering is critically dependent on the dimensions of its peptide-MHC ligand. Nature 436, 578-582.

Cochran, J.R., Cameron, T.O., and Stern, L.J. (2000). The relationship of MHC-peptide binding and T cell activation probed using chemically defined MHC class II oligomers. Immunity 12, 241-250.

Contreras, F.X., Ernst, A.M., Haberkant, P., Bjorkholm, P., Lindahl, E., Gonen, B., Tischer, C., Elofsson, A., von Heijne, G., Thiele, C., et al. (2012). Molecular recognition of a single sphingolipid species by a protein's transmembrane domain. Nature 481, 525-529.

Coskun, U., Grzybek, M., Drechsel, D., and Simons, K. (2011). Regulation of human EGF receptor by lipids. Proc Natl Acad Sci U S A 108, 9044-9048.

Coskun, U., and Simons, K. (2011). Cell membranes: the lipid perspective. Structure 19, 1543-1548.

Davis, M.M., Boniface, J.J., Reich, Z., Lyons, D., Hampl, J., Arden, B., and Chien, Y. (1998). Ligand recognition by αβ T cell receptors. Annu. Rev. Immunol. 16, 523-544.

Davis, S.J., and van der Merwe, P.A. (2006). The kinetic-segregation model: TCR triggering and beyond. Nat. Immunol. 7, 803-809.

de la Cruz, J., Kruger, T., Parks, C.A., Silge, R.L., van Oers, N.S., Luescher, I.F., Schrum, A.G., and Gil, D. (2011). Basal and antigen-induced exposure of the proline-rich sequence in CD3ε. J. Immunol. 186, 2282-2290.

Deswal, S., Schulze, A.K., Hofer, T., and Schamel, W.W. (2011). Quantitative analysis of protein phosphorylations and interactions by multi-colour IP-FCM as an input for kinetic modelling of signalling networks. PLoS One 6, e22928.

Fahmy, T.M., Bieler, J.G., Edidin, M., and Schneck, J.P. (2001). Increased TCR avidity after T cell activation: a mechanism for sensing low-density antigen. Immunity 14, 135-143.

Falck, E., Patra, M., Karttunen, M., Hyvonen, M.T., and Vattulainen, I. (2004). Lessons of slicing membranes: interplay of packing, free area, and lateral diffusion in phospholipid/cholesterol bilayers. Biophys. J. 87, 1076-1091.

Gil, D., Schamel, W.W., Montoya, M., Sanchez-Madrid, F., and Alarcon, B. (2002). Recruitment of Nck by CD3 epsilon reveals a ligand-induced conformational change essential for T cell receptor signaling and synapse formation. Cell 109, 901-912.

Gimpl, G., and Gehrig-Burger, K. (2007). Cholesterol reporter molecules. Biosci. Rep. 27, 335-358.

Hanson, M.A., Cherezov, V., Griffith, M.T., Roth, C.B., Jaakola, V.P., Chien, E.Y., Velasquez, J., Kuhn, P., and Stevens, R.C. (2008). A specific cholesterol binding site is established by the 2.8 A structure of the human beta2-adrenergic receptor. Structure 16, 897-905.

Horejsi, V. (2003). The roles of membrane microdomains (rafts) in T cell activation. Immunol. Rev. 191, 148-164.

Iwashima, M., Irving, B.A., van Oers, N.S., Chan, A.C., and Weiss, A. (1994). Sequential interactions of the TCR with two distinct cytoplasmic tyrosine kinases. Science 263, 1136-1139.

James, J.R., and Vale, R.D. (2012). Biophysical mechanism of T-cell receptor triggering in a reconstituted system. Nature 487, 64-69.

Kabouridis, P.S., Janzen, J., Magee, A.L., and Ley, S.C. (2000). Cholesterol depletion disrupts lipid rafts and modulates the activity of multiple signaling pathways in T lymphocytes. Eur. J. Immunol. 30, 954-963.

Kaech, S.M., Hemby, S., Kersh, E., and Ahmed, R. (2002). Molecular and functional profiling of memory CD8 T cell differentiation. Cell 111, 837-851.

Kim, J.E., and White, F.M. (2006). Quantitative analysis of phosphotyrosine signaling networks triggered by CD3 and CD28 costimulation in Jurkat cells. J. Immunol. 176, 2833-2843.

Kim, S.T., Takeuchi, K., Sun, Z.Y., Touma, M., Castro, C.E., Fahmy, A., Lang, M.J., Wagner, G., and Reinherz, E.L. (2009). The alphabeta T cell receptor is an anisotropic mechanosensor. J. Biol. Chem. 284, 31028-31037.

Krogsgaard, M., Li, Q.J., Sumen, C., Huppa, J.B., Huse, M., and Davis, M.M. (2005). Agonist/endogenous peptide-MHC heterodimers drive T cell activation and sensitivity. Nature 434, 238-243.

Kuhns, M.S., and Davis, M.M. (2012). TCR signaling emerges from the sum of many parts. Front. Immunol. 3, 159.

Kumar, R., Ferez, M., Swamy, M., Arechaga, I., Rejas, M.T., Valpuesta, J.M., Schamel, W.W., Alarcon, B., and van Santen, H.M. (2011). Increased Sensitivity of Antigen-Experienced T Cells through the Enrichment of Oligomeric T Cell Receptor Complexes. Immunity 35, 375-387.

Lee, M.S., Glassman, C.R., Deshpande, N.R., Badgandi, H.B., Parrish, H.L., Uttamapinant, C., Stawski, P.S., Ting, A.Y., and Kuhns, M.S. (2015). A Mechanical Switch Couples T Cell Receptor Triggering to the Cytoplasmic Juxtamembrane Regions of CD3zetazeta. Immunity 43, 227-239.

Martinez-Martin, N., Risueno, R.M., Morreale, A., Zaldivar, I., Fernandez-Arenas, E., Herranz, F., Ortiz, A.R., and Alarcon, B. (2009). Cooperativity between T cell receptor complexes revealed by conformational mutants of CD3epsilon. Sci. Signal 2, ra43.

Mingueneau, M., Sansoni, A., Gregoire, C., Roncagalli, R., Aguado, E., Weiss, A., Malissen, M., and Malissen, B. (2008). The proline-rich sequence of CD3epsilon controls T cell antigen receptor expression on and signaling potency in preselection CD4+CD8+ thymocytes. Nat. Immunol. 9, 522-532.

Minguet, S., and Schamel, W.W.A. (2008). A permissive geometry model for TCR-CD3 activation. Trends Biochem. Sci. 33, 51-57.

Minguet, S., Swamy, M., Alarcon, B., Luescher, I.F., and Schamel, W.W. (2007). Full activation of the T cell receptor requires both clustering and conformational changes at CD3. Immunity 26, 43-54.

Molnar, E., Swamy, M., Holzer, M., Beck-Garcia, K., Worch, R., Thiele, C., Guigas, G., Boye, K., Luescher, I.F., Schwille, P., et al. (2012). Cholesterol and sphingomyelin drive ligand-independent T-cell antigen receptor nanoclustering. J. Biol. Chem. 287, 42664-42674.

Monod, J., Wyman, J., and Changeux, J.P. (1965). On the nature of allosteric transitions: a plausible model. J. Molec. Biol. 12, 88-118.

Montixi, C., Langlet, C., Bernard, A.M., Thimonier, J., Dubois, C., Wurbel, M.A., Chauvin, J.P., Pierres, M., and He, H.T. (1998). Engagement of T cell receptor triggers its recruitment to low-density detergent-insoluble membrane domains. EMBO J. 17, 5334-5348.

Nika, K., Soldani, C., Salek, M., Paster, W., Gray, A., Etzensperger, R., Fugger, L., Polzella, P., Cerundolo, V., Dushek, O., et al. (2010). Constitutively active Lck kinase in T cells drives antigen receptor signal transduction. Immunity 32, 766-777.

O'Shea, J.J., McVicar, D.W., Bailey, T.L., Burns, C., and Smyth, M.J. (1992). Activation of human peripheral blood T lymphocytes by pharmacological induction of protein-tyrosine phosphorylation. Proc. Natl. Acad. Sci. U S A 89, 10306-10310.

Petersen, T.R., Gulland, S., Bettelli, E., Kuchroo, V., Palmer, E., and Backstrom, B.T. (2004). A chimeric T cell receptor with super-signaling properties. Int. Immunol. 16, 889-894.

Potter, T.A., Rajan, T.V., Dick, R.F., 2nd, and Bluestone, J.A. (1989). Substitution at residue 227 of H-2 class I molecules abrogates recognition by CD8-dependent, but not CD8-independent, cytotoxic T lymphocytes. Nature 337, 73-75.

Risueno, R.M., Gil, D., Fernandez, E., Sanchez-Madrid, F., and Alarcon, B. (2005). Ligand-induced conformational change in the T-cell receptor associated with productive immune synapses. Blood 106, 601-608.

Risueno, R.M., Schamel, W.W., and Alarcon, B. (2008). T cell receptor engagement triggers its CD3epsilon and CD3zeta subunits to adopt a compact, locked conformation. PLoS One 3, e1747.

Rouquette-Jazdanian, A.K., Pelassy, C., Breittmayer, J.P., and Aussel, C. (2006). Revaluation of the role of cholesterol in stabilizing rafts implicated in T cell receptor signaling. Cell Signal. 18, 105-122.

Schamel, W.W., Arechaga, I., Risueno, R.M., van Santen, H.M., Cabezas, P., Risco, C., Valpuesta, J.M., and Alarcon, B. (2005). Coexistence of multivalent and monovalent TCRs explains high sensitivity and wide range of response. J. Exp. Med. 202, 493-503.

Shi, X., Bi, Y., Yang, W., Guo, X., Jiang, Y., Wan, C., Li, L., Bai, Y., Guo, J., Wang, Y., et al. (2013). Ca2+ regulates T-cell receptor activation by modulating the charge property of lipids. Nature 493, 111-115.

Steinberg, M., Adjali, O., Swainson, L., Merida, P., Di Bartolo, V., Pelletier, L., Taylor, N., and Noraz, N. (2004). T-cell receptor-induced phosphorylation of the zeta chain is efficiently promoted by ZAP-70 but not Syk. Blood 104, 760-767.

Tani-ichi, S., Maruyama, K., Kondo, N., Nagafuku, M., Kabayama, K., Inokuchi, J., Shimada, Y., Ohno-Iwashita, Y., Yagita, H., Kawano, S., and Kosugi, A. (2005). Structure and function of lipid rafts in human activated T cells. Int. Immunol. 17, 749-758.

Thiele, C., Hannah, M.J., Fahrenholz, F., and Huttner, W.B. (2000). Cholesterol binds to synaptophysin and is required for biogenesis of synaptic vesicles. Nat. Cell Biol. 2, 42-49.

van der Merwe, P.A., and Dushek, O. (2011). Mechanisms for T cell receptor triggering. Nat Rev. Immunol. 11, 47-55.

Xavier, R., Brennan, T., Li, Q., McCormack, C., and Seed, B. (1998). Membrane compartmentation is required for efficient T cell activation. Immunity 8, 723-732.

Xu, C., Gagnon, E., Call, M.E., Schnell, J.R., Schwieters, C.D., Carman, C.V., Chou, J.J., and Wucherpfennig, K.W. (2008). Regulation of T cell receptor activation by dynamic membrane binding of the CD3ε cytoplasmic tyrosine-based motif. Cell 135, 702-713.

FIGURE LEGENDS

Figure 1. Active TCRs cannot bind to cholesterol

(A) Cholesterol only binds to the inactive TCR (TCR_I, upper panel). Active TCRs (TCR_A) accumulate when bound to anti-CD3, anti-TCR or pMHC and do not bind to cholesterol (lower panel). Radioactive photocholesterol can be covalently cross-linked to TCRβ upon UV light exposure.

(B) Jurkat cells were grown with photocholesterol, and were either UV-irradiated and then stimulated with anti-CD3ε (OKT3) for the indicated times at 37°C (-); or stimulated first and then UV-irradiated (+). Protein G-beads were added to the lysate to capture antibody-bound TCRs. Purified proteins were separated by SDS-PAGE and autoradiography and WB were performed. For quantification, the intensity of the radioactive band corresponding to cholesterol-bound TCRβ was divided by the intensity of the anti-CD3ζ WB, the different time points were pooled, n=6. $p<0.01$ by two-sided one-sample t-test.

(C) Jurkat cells were stimulated as in (B) and the SH3-PD assay was performed. SH3-bound proteins and the lysates were analyzed by WB. SH3-GST serves as a bead loading control. The intensity of CD3ζ in the SH3-PD was normalized to the SH3-GST signal in the PD pooled from different time points, n=4, $p<0.05$ by two-sided one-sample t-test.

(D) In the cholesterol-PD assay, only TCR_I binds to cholesterol-coupled beads.

(E) Jurkat cells were left untreated or stimulated with anti-TCRβ (Jovi1) or anti-CD3ε at 37°C for 5 min or at 0°C in the presence of PP2 for 2 hours. Lysates and the proteins purified upon the cholesterol- and SH3-PD were visualized by WB, n=5.

(F) WB signals of cholesterol- and stearate-PD assays were quantified, normalized, and the relative amounts of TCRs bound to the lipid (lipid-PD assay, CD3ε/Bub3) are plotted versus the normalized, relative amount of TCR_A (SH3-PD assay, ζ/SH3-GST). The quantification of 4-8 experiments assaying TCR binding to lipid and of 3-6 experiments assaying the TCR

conformational state were pooled. p-value indicates whether the slope calculated through linear regression is significantly non-zero.

(G) In contrast to the wt TCR, the K76T TCR does not switch to TCR_A.

(H) Jurkat cells expressing wt or K76T murine CD3ε were stimulated with anti-murine CD3ε (145-2C11) for 5 min and the cholesterol-PD assay was performed. Quantification (n=5) is shown on the right, *p<0.05 by two-sided one-sample t-test.

Figure 2. A mutant TCR with reduced cholesterol binding switches to the TCR_A state

(A) wt TCRs bind cholesterol via the TCRβ TM region. The TMchim TCR is composed of the ectodomains of TCRβ and the TM region of TCRγ2 (orange) and does not bind cholesterol.

(B) wt scTCRβ- and TMchim scTCR-expressing cells were left untreated or stimulated with anti-CD3ε (OKT3) for 5 min and the cholesterol-PD assay was performed as in Figure 1E (n=4).

(C) Cells treated as in (B) were subjected to the SH3-PD assay as Figure 1E (n=3).

(D) Cells treated as in (B) were lysed, an IP using OKT3 and WB were done as indicated. The ratios of the band intensities of phospho-ζ/ε (n=4-9) and phospho-ε/ε (n=4-11) obtained from the TMchim TCR were normalized to the corresponding ratio obtained from the wt TCR, ***p<0.001 by two-sided one-sample t-test.

(E) Cells were treated as in (B) and analyzed for phospho-Erk and Erk by WB (n=5).

Figure 3. Cholesterol prevents spontaneous signaling

(A) Cholesterol removal from the TCR results in switching to the TCR_A state and thereby to spontaneous signaling.

(B) Jurkat cells were left untreated or incubated with cholesterol oxidase for 1 hour. After

lysis, an SH3-PD and anti-CD3ε IP were performed. Purified proteins and the lysate were analyzed by WB. The band intensities (n=4) were quantified and plotted normalized to the non-treated cells (TCR_A: ζ (SH3-PD)/SH3-GST / ζ (IP); phospho-Erk: phoshpo-Erk (lysate) / ζ (lysate)), *p<0.05, ** p<0.01 by two-sided one-sample t-test.

(C) Jurkat cells were treated with cholesterol oxidase for 5 min at 37°C or left untreated and lysed. TCRs were purified by an anti-CD3ε IP. WB was done as indicated. The band intensities were quantified and plotted as phospho-CD3ζ / CD3ε (n=3), *p<0.05 by two-sided one-sample t-test.

(D) TCRβ-negative Jurkat cells were treated as in (B) and the amount of phospho-Erk was quantified as in (B) (n=3).

Figure 4. In living cells cholesterol-bound TCRs cannot be phosphorylated

(A, B) Jurkat cells grown in radioactive photo-cholesterol (red star) were either first exposed to UV light and then stimulated with pervanadate (lane 1), or first stimulated with pervanadate and then exposed to UV light (lane 2). The cells also contain endogenous cholesterol that cannot be cross-linked to the TCR (depicted without the star). After cell lysis, only phosphorylated TCRs were purified using an anti-phospho-tyrosine beads. Proteins were separated by reducing SDS-PAGE and an autoradiography and WB was done (n=2).

(C) Jurkat cells were left untreated or stimulated with pervanadate. The lysate was split into 3 parts; the cholesterol- and SH3-PD assays were performed (top and middle panels), and the lysates were analysed (lower panels) (n=3).

(D) TCRs are in equilibrium between the inactive (TCR_I, blue), active (TCR_A, red) and phosphorylated states. In resting cells, the TCR_I state and phosphatase activity dominate, so that most TCRs are non-phosphorylated. The K76T TCR cannot switch to TCR_A.

(E) Jurkat cells expressing wt or K76T murine CD3ε were stimulated with pervanadate. Cell numbers were adjusted to the same amount of murine CD3ε molecule numbers on the cell surface. After lysis, TCRs were isolated with anti-mouse CD3ε antibodies. WB was done as indicated (n=3).

Figure 5. Only TCR_A is accessible to be phosphorylated by kinases

(A) TCR_I is not amenable to phosphorylation by active Lck. Ligand stabilizes TCR_A, so that it can be phosphorylated by Lck.

(B) Buffer alone (-), anti-CD3ε or anti-TCRβ were added to scTCRs bound to nitro-phenol-coupled beads. After further addition of recombinant active Lck and ATP, the kinase reaction was incubated at 37°C for 30 minutes. The WB was developed with anti-phospho-tyrosine (4G10, visualizing phospho-Lck), pan anti-phospho-CD3ζ, anti-phospho-εY1, and anti-CD3ε. The SH3-PD assay was performed in parallel.

(C) Quantification of the amounts of phospho-CD3ζ (n=5) and phospho-εY1 (n=7) relative to CD3ε and normalized to unstimulated condition is shown, ** $p < 0.01$, *** $p < 0.001$ by two-sided one-sample t-test.

(D) Membrane patches of scTCRβ cells were treated with anti-CD3ε antibodies or left untreated. Samples were treated as in B (n=2).

(E) Cholesterol was added to purified scTCRs (chol) or not (-). Then, anti-CD3ε antibodies were given and the SH3-PD was performed (n=3). In parallel, protein G-coupled sepharose was added and purified TCRs analyzed by WB.

(F) A reconstituted CD3 phosphorylation reaction was done as in (B), in the presence or absence of cholesterol (n=3).

Figure 6. A lipid-regulated allosteric model for TCR triggering

(A) On resting T cells, most TCRs adopt the inactive conformation, of those 50% are bound to cholesterol ($TCR_{I,c}$) and 50% are not ($TCR_{I,-}$). Only $TCR_{I,-}$ spontaneously switches to TCR_A. Monovalent pMHC binds equally well to both TCR_I and TCR_A. The allosteric switch to TCR_A allows pMHC dimers with a permissive geometry to bind bivalently, stabilizing TCR_A. Only TCR_A can be phosphorylated.

(B) After anti-CD3ε stimulation the percentage of TCR_A was measured experimentally by the SH3-PD assay for the wt and the TMchim TCR (black dots, n=4) or predicted from the model (red dots).

(C) Lymph node cells of OT-1 TCRαβ transgenic mice expressing wt (red) or C80G CD3ε (a mutant that cannot switch to TCR_A, green) were stained on ice for 30 min with increasing concentrations of PE-labeled OVA-D227K-H2-K^b tetramers and with an APC-labeled anti-CD3 antibody (17A2) and measured by flow cytometry. We gated on cells with similar TCR-expression levels. The MFI values of the bound tetramer were normalized to the amount of surface TCR (n=3), * $p < 0.05$, *** $p < 0.001$ by unpaired t-test. The best fit of the model to the experimental data is shown by solid lines, the 95% confidence intervals of the fit as colored areas.

(D) Dose-response curves of the fraction of TCR_A as a function of the concentration of D227K-pMHC tetramer (left) and as a function of cholesterol concentration (right) were calculated by the model. Parameters as in Figure S6B.

(E) Dose-response curves of the fraction of bound D22K-pMHC tetramer as a function of the cholesterol concentration were calculated by the model. Parameters are as in Figure S6B.

Figure 1

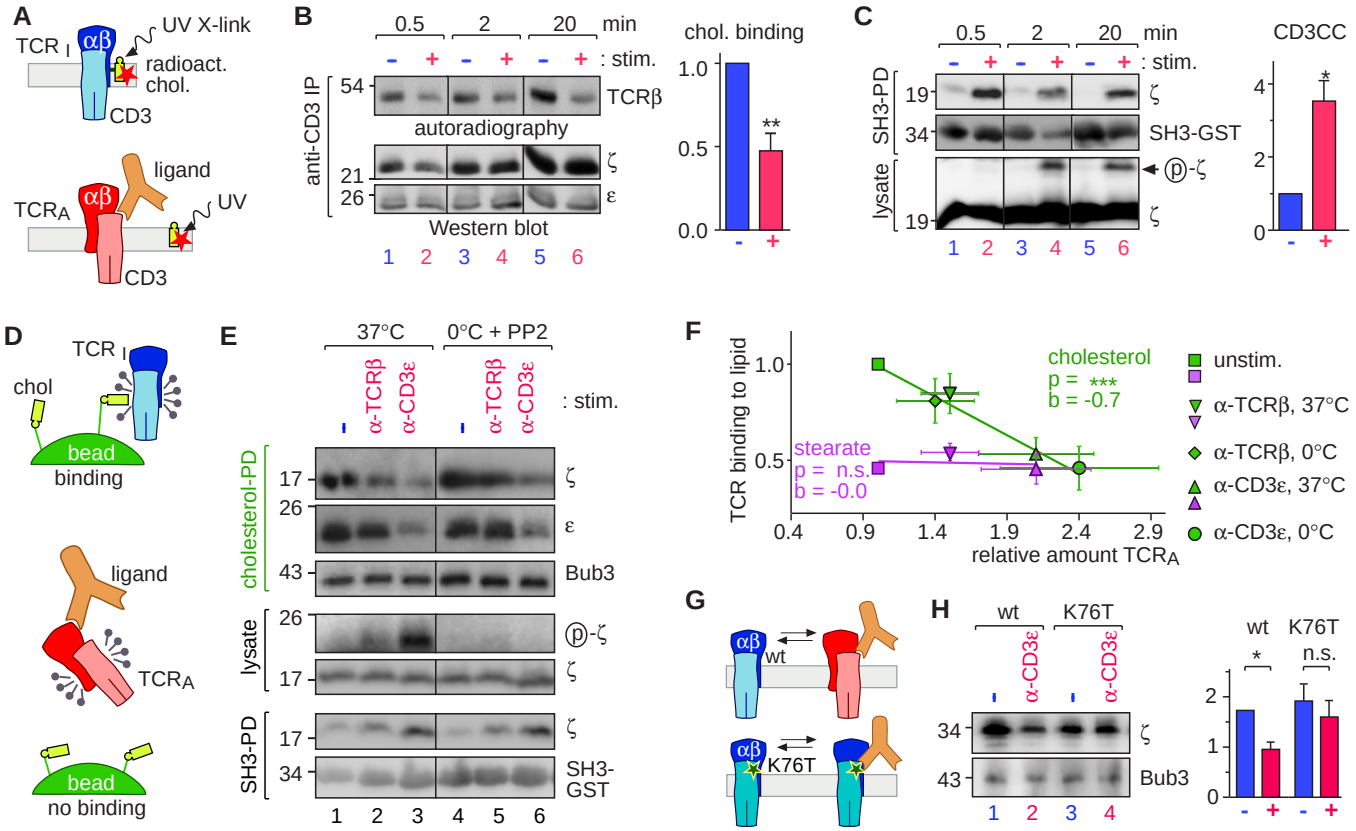
A
TCR
αβ
UV X-link
radioact. chol.
CD3
ligand
TCRA
UV
B
0.5
2
20
min
: stim.
anti-CD3 IP
54
TCRβ
autoradiography
21
26
ζ
ε
Western blot
1 2 3 4 5 6
chol. binding
1.0
0.5
0.0
**
C
SH3-PD
19
34
SH3-GST
lysate
ⓟ-ζ
CD3CC
*
D
chol
bead
binding
no binding
E
37°C
0°C + PP2
α-TCRβ
α-CD3ε
cholesterol-PD
17
26
43
Bub3
lysate
SH3-PD
SH3-GST
F
TCR binding to lipid
cholesterol
p = ***
b = -0.7
stearate
p = n.s.
b = -0.0
relative amount TCRA
unstim.
α-TCRβ, 37°C
α-TCRβ, 0°C
α-CD3ε, 37°C
α-CD3ε, 0°C
G
wt
K76T
H
wt
K76T
n.s.

Figure 2

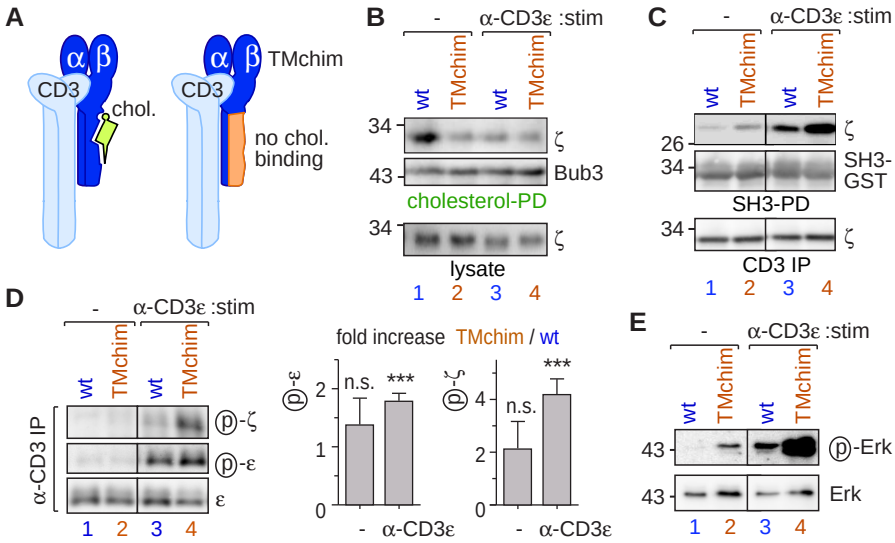
A
CD3
chol.
CD3
TMchim
no chol.
binding
B
-
α-CD3ε :stim
wt
TMchim
wt
TMchim
34
ζ
43
Bub3
cholesterol-PD
34
ζ
lysate
1 2 3 4
C
-
α-CD3ε :stim
wt
TMchim
wt
TMchim
26
34
ζ
SH3-
GST
SH3-PD
34
ζ
CD3 IP
1 2 3 4
D
-
α-CD3ε :stim
wt
TMchim
wt
TMchim
α-CD3 IP
ⓟ-ζ
ⓟ-ε
ε
1 2 3 4
fold increase TMchim / wt
ⓟ-ε
n.s.
***
2
1
0
- α-CD3ε
ⓟ-ζ
n.s.
***
4
2
0
- α-CD3ε
E
-
α-CD3ε :stim
wt
TMchim
wt
TMchim
43
ⓟ-Erk
43
Erk
1 2 3 4

Figure 3

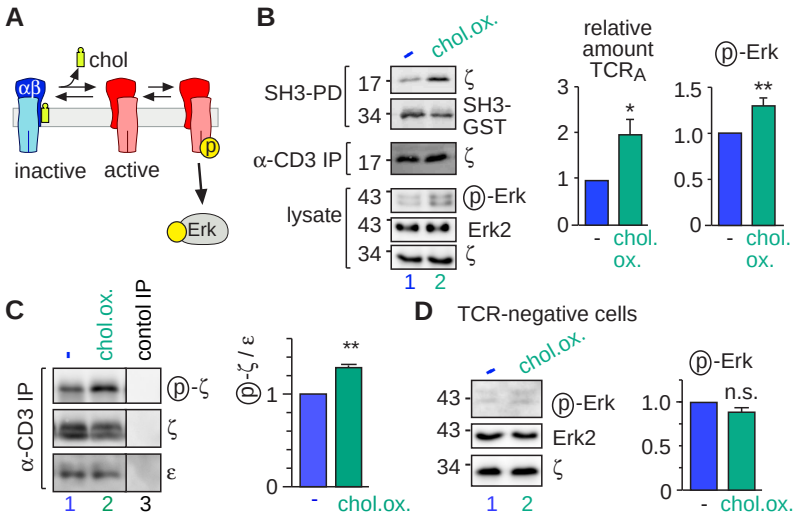
A
chol
αβ
inactive
active
p
Erk
B
chol.ox.
SH3-PD
17
ζ
34
SH3-GST
α-CD3 IP
17
ζ
lysate
43
ⓟ-Erk
43
Erk2
34
ζ
1 2
relative amount TCRA
3
2
1
0
*
- chol. ox.
ⓟ-Erk
1.5
1.0
0.5
0
**
- chol. ox.
C
chol.ox.
contol IP
α-CD3 IP
ⓟ-ζ
ζ
ε
1 2 3
ⓟ-ζ / ε
1
0
**
- chol.ox.
D
TCR-negative cells
chol.ox.
43
ⓟ-Erk
43
Erk2
34
ζ
1 2
ⓟ-Erk
1.0
0.5
0
n.s.
- chol.ox.

Figure 4

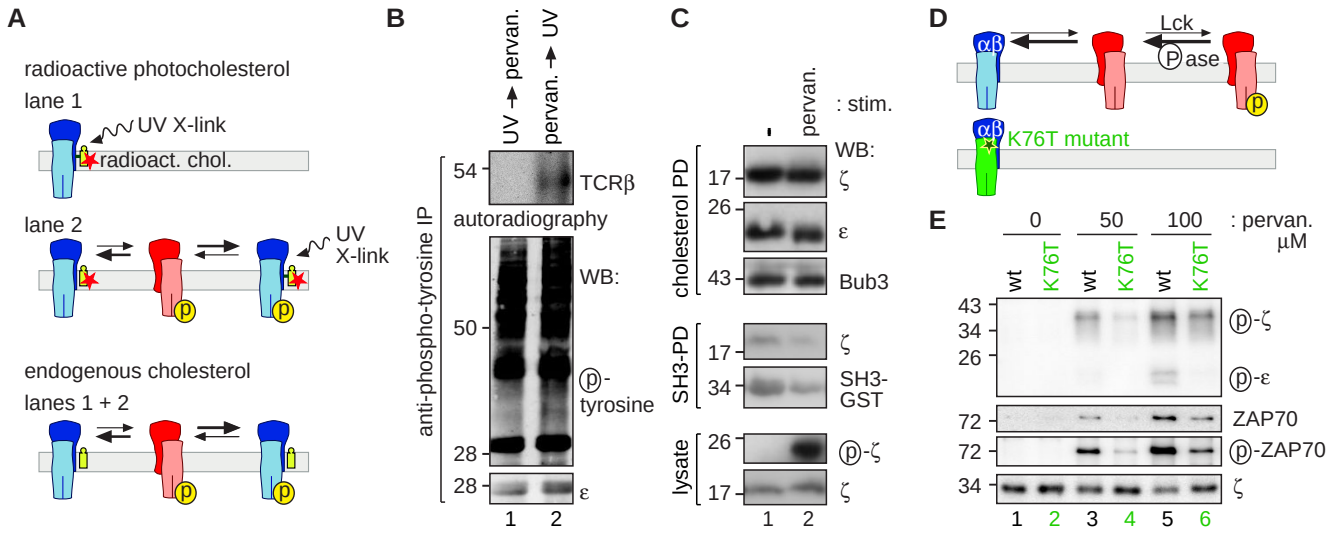
A
radioactive photocholesterol
lane 1
UV X-link
radioact. chol.
lane 2
UV
X-link
endogenous cholesterol
lanes 1 + 2
B
UV → pervan.
pervan. → UV
anti-phospho-tyrosine IP
54
TCRβ
autoradiography
WB:
50
ⓟ-
tyrosine
28
28
ε
1 2
C
pervan.
: stim.
WB:
cholesterol PD
17
ζ
26
ε
43
Bub3
SH3-PD
17
ζ
34
SH3-
GST
lysate
26
ⓟ-ζ
17
ζ
1 2
D
Lck
Pase
αβ
K76T mutant
E
0
50
100
: pervan.
μM
wt
K76T
wt
K76T
wt
K76T
43
34
26
ⓟ-ζ
ⓟ-ε
72
ZAP70
72
ⓟ-ZAP70
34
ζ
1 2 3 4 5 6

Figure 5

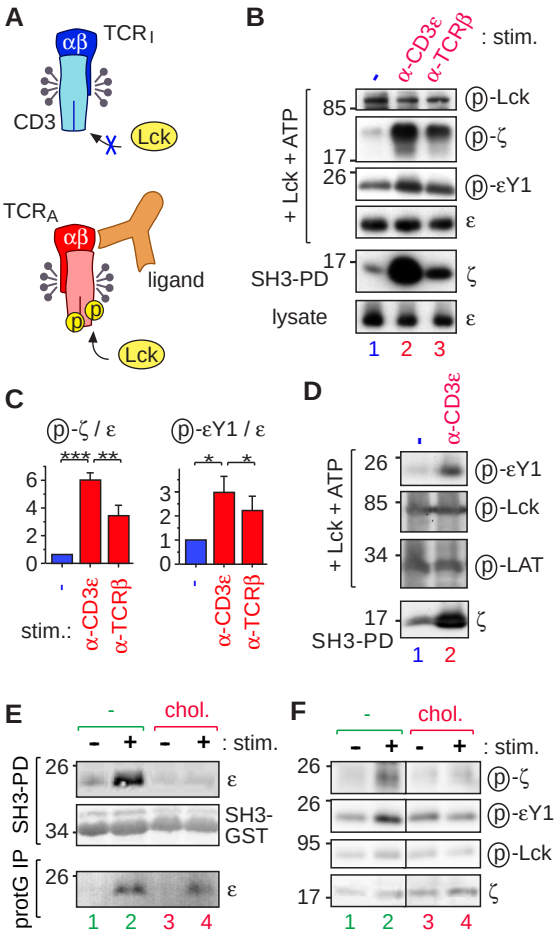
A
TCRI
αβ
CD3
Lck
TCRA
αβ
ligand
p
Lck
B
: stim.
α-CD3ε
α-TCRβ
+ Lck + ATP
85
17
26
ⓟ-Lck
ⓟ-ζ
ⓟ-εY1
ε
SH3-PD
17
ζ
lysate
ε
1 2 3
C
ⓟ-ζ / ε
ⓟ-εY1 / ε
***
**
*
*
6
4
2
0
3
2
1
0
stim.:
α-CD3ε
α-TCRβ
D
α-CD3ε
+ Lck + ATP
26
85
34
ⓟ-εY1
ⓟ-Lck
ⓟ-LAT
17
SH3-PD
ζ
1 2
E
-
chol.
- + - + : stim.
SH3-PD
26
34
ε
SH3-GST
protG IP
26
ε
1 2 3 4
F
-
chol.
- + - + : stim.
26
26
95
17
ⓟ-ζ
ⓟ-εY1
ⓟ-Lck
ζ
1 2 3 4

Figure 6

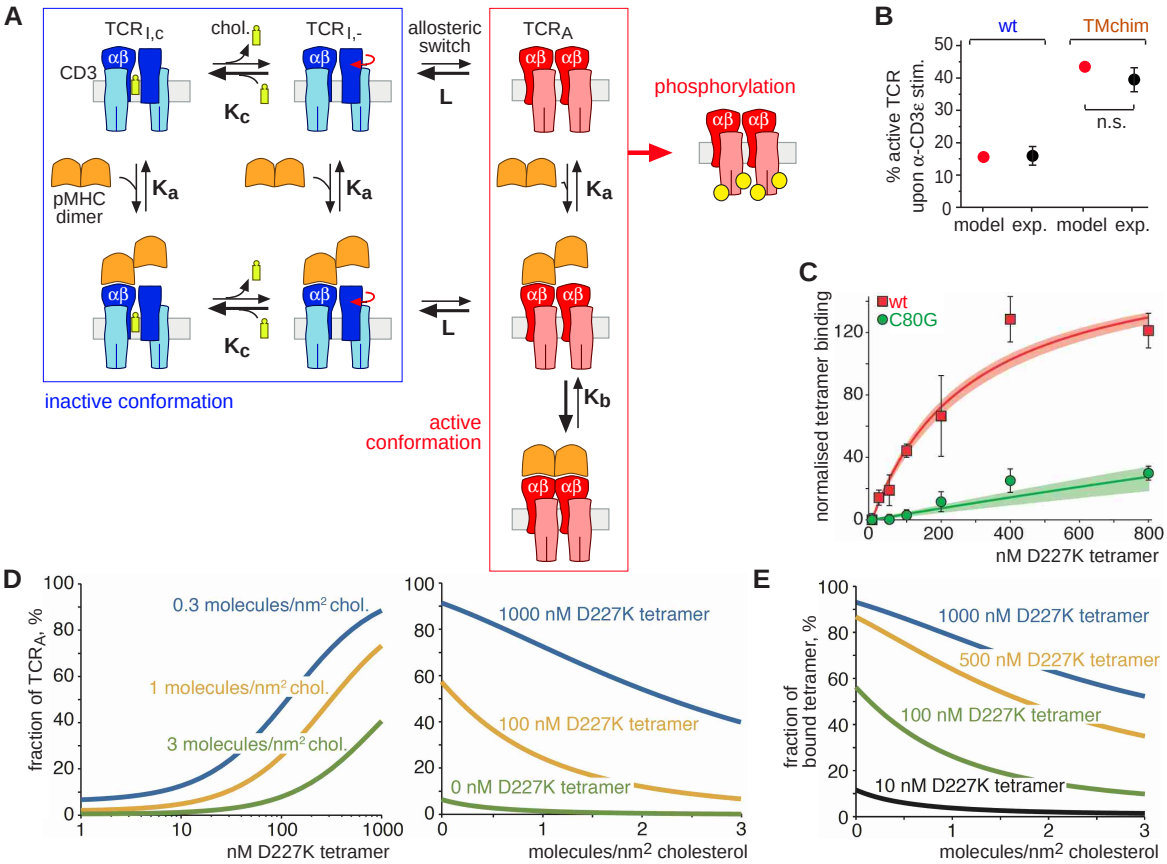
A
TCR l,c
chol.
TCR l,-
CD3
αβ
Kc
allosteric switch
L
TCRA
pMHC dimer
Ka
Kb
inactive conformation
active conformation
phosphorylation
B
wt
TMchim
% active TCR upon α-CD3ε stim.
n.s.
model exp. model exp.
C
wt
C80G
normalised tetramer binding
nM D227K tetramer
D
fraction of TCRA, %
0.3 molecules/nm² chol.
1 molecules/nm² chol.
3 molecules/nm² chol.
nM D227K tetramer
1000 nM D227K tetramer
100 nM D227K tetramer
0 nM D227K tetramer
molecules/nm² cholesterol
E
fraction of bound tetramer, %
1000 nM D227K tetramer
500 nM D227K tetramer
100 nM D227K tetramer
10 nM D227K tetramer
molecules/nm² cholesterol

SUPPLEMENTAL INFORMATION

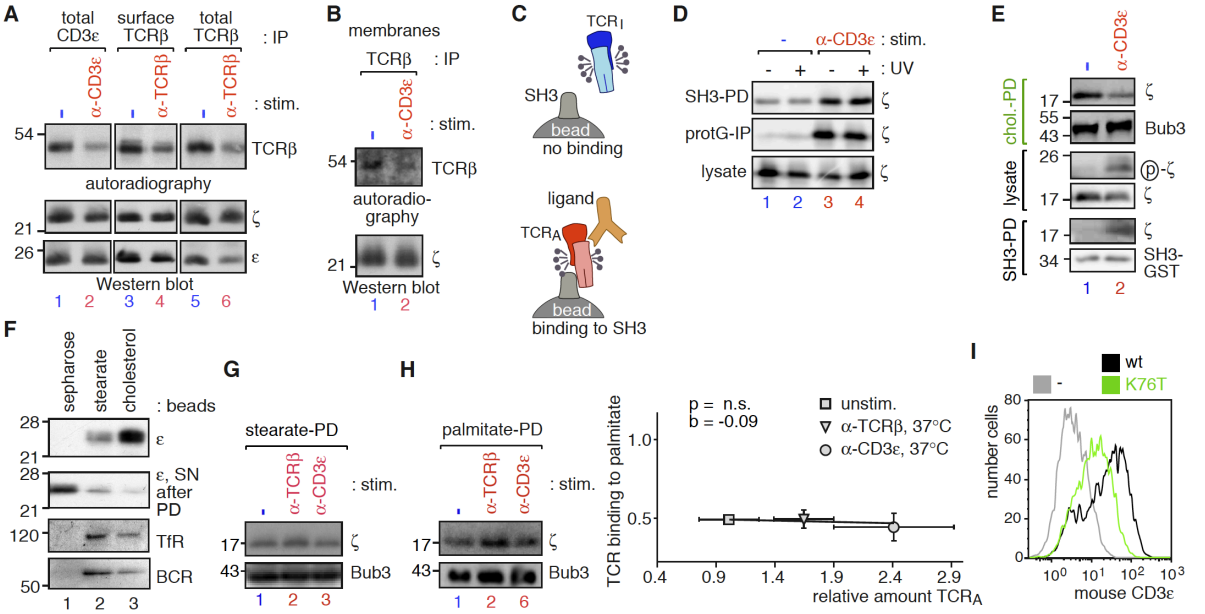

Figure S1. Active TCRs do not bind to cholesterol, Related to Figure 1

(A) Jurkat cells were grown with radioactive photocholesterol, and were either exposed to UV light and then treated with anti-CD3ε (UCHT1) or anti-TCRβ (Jovi1) antibodies for 20 min at 37°C (-); or stimulated first and then exposed to UV light (α-CD3ε, α-TCRβ). After cell lysis, additional anti-CD3ε or anti-TCRβ antibodies were added, to immunoprecipitate all TCRs using protein G-sepharose beads (lanes, 1, 2, 5, 6). Alternatively, protein G-sepharose beads alone were added, in order to capture the antibody-bound cell surface TCRs (lanes 3, 4). Purified proteins were separated and analysed as is Figure 1B.

(B) Jurkat cells were grown with radioactive photocholesterol and membranes patches were prepared as described in Supplemental Experimental Procedure. Stimulation and analysis were done as in A.

(C) The SH3-PD is graphically depicted. In the TCR_I state (blue), the CD3ε proline rich sequence is not available for binding to the GST-coupled Nck SH3.1 domain bound to glutathione beads. In contrast, antibody- or pMHC-stimulated TCRs are in the active conformation (TCR_A, red), allowing the proline-rich sequence to bind to the SH3-bound beads.

(D) Jurkat cells grown without photocholesterol were left unstimulated or treated with anti-CD3ε antibodies for 2 hours at 4°C. Subsequently, cells were UV irradiated or not. The SH3-PD assay and a protein G-coupled sepharose IP were performed. Purified proteins and the lysate were analysed. The data show that irradiation with UV light per se did not affect the conformational state of the TCR.

(E) Human peripheral blood mononuclear cells (PBMCs) from a healthy donor were left unstimulated (-) or treated for 5 min at 37°C with anti-CD3ε (UCHT1). The cholesterol- and SH3-PD assays were performed as in Figure 1E.

(F) The TCR and the transferrin receptor (TfR) were purified from M.mζ-SBP and M.hTfR-SBP cells through the streptavidin-binding peptide (SBP) with streptavidin-coupled beads and then eluted with 4 mM biotin. The BCR was purified from J558Lmb1/δm B cells with nitro-phenol-coupled beads and eluted with 5 mM nitro-iodo-phenol. The eluates were subjected to a lipid-PD assay with uncoupled, stearate- or cholesterol-coupled sepharose beads and the bound proteins detected by WB. In the second row, the supernatant after the PD was analysed, showing that most, if not all, resting TCRs possess the capacity to bind to cholesterol.

(G) Jurkat cells were stimulated as described in Figure 1E. After lysis, a PD assay with stearate- coupled beads was performed and analysed as in Figure 1E top panels.

(H) An experiment as in Figure S1G using palmitate-coupled beads was performed and analysed as in Figure 1F. We conclude that the palmitate-TCR interaction is not influenced by the conformational state of the TCR.

(I) Mouse CD3ε in its wild type (wt) and mutant K76T forms were lentivirally expressed in human Jurkat cells. Cells were stained with the anti-mouse CD3ε antibody 145-2C11. The flow cytometric analysis shows that the K76T TCR (green) has an approximately two-fold reduced surface expression compared to the wt TCR (black) as already reported when expressed in murine T cells (Martinez-Martin et al., 2009). The parental Jurkat cells did not express any mouse CD3ε chains (grey).

This figure corroborates the finding that stimulated TCRs (whether expressed in Jurkat cells or in primary human T cells) lose their capacity to bind to cholesterol. In contrast, the binding of the TCR to stearate and palmitate was not altered by stimulation.

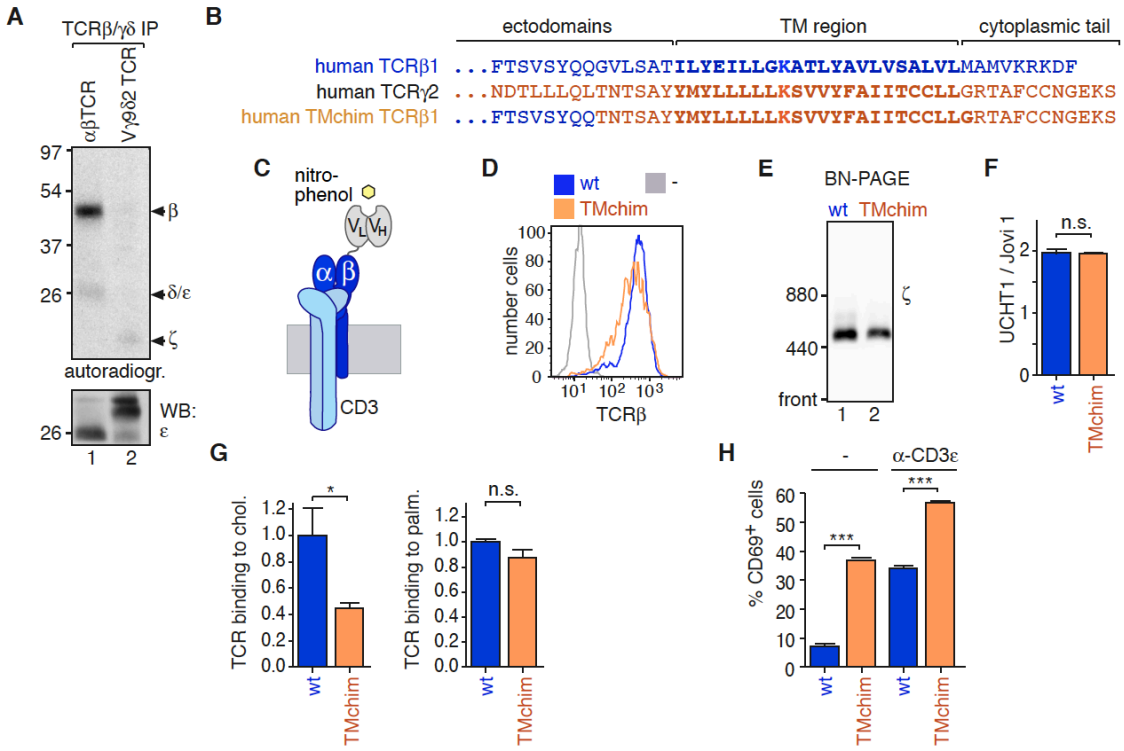

Figure S2. Analysis of the TMchim TCR, Related to Figure 2

(A) Jurkat cells expressing the αβTCR (lane 1) or the human Vγ9Vδ2 TCR (lane 2) were cultured for 16 h with 200 µCi/ml photocholesterol, and the diazirin group was activated by UV light. After lysis, TCRs were immunoprecipitated (IP) using anti-TCRβ or anti-TCRγδ antibodies and separated by reducing SDS-PAGE. The autoradiogram (top) and anti-CD3ε WB (bottom) are shown.

(B) The amino acid sequences of the TM and cytoplasmic regions of human TCRβ1, human TCRγ2 and the TMchim TCRβ chain are shown. Annotation of the TM regions was done according to (Backstrom et al., 1996; Petersen et al., 2004).

(C) The scTCR contains the scTCRβ chain that is composed of a single chain (sc) construct of the variable immunoglobulin (Ig) domains of a nitro-phenol (NP)-specific antibody (scFv) connected by a linker of 8 amino acids to the N terminus of wt TCRβ (Minguet et al., 2007). NP binding to the scTCR does not influence the conformational state of the TCR (Minguet et al., 2007).

(D) wt scTCRβ and TMchim scTCRβ-expressing cells were stained with anti-human TCRβ (Jovi3) and PE-coupled anti-mouse IgG. Both scTCRβ chains (wt blue, TMchim orange) are expressed on the cell surface to equal levels. The parental 31-13 cells did not express any TCRβ chain (grey).

(E) wt scTCRβ and TMchim scTCRβ were expressed in the TCRβ-deficient 31-13 Jurkat-derived cell line. These cells were lysed in 1% digitonin, the scTCR was affinity-purified by NP-sepharose beads and eluted using 5 mM free NIP. After separation by BN-PAGE, WB was done with an anti-CD3ζ antibody, showing that the TMchim TCR had the same size as the wt TCR. This suggested that the stoichiometry was the same in both TCRs.

(F) Wt TCR and TMchim TCR-expressing cells were stained with the antibody Jovi1 that recognizes the constant Ig domain of TCRβ, but only when this domain is folded correctly (Huppa and Ploegh, 1997), and with the anti-CD3 antibody UCHT1 which only recognizes folded CD3ε (Arnett et al., 2004). A FITC-labelled secondary antibody recognizing Jovi1 and UCHT1 was used and the fluorescence intensity was measured by flow cytometry. Staining with the secondary antibody alone served to substract the background staining intensity. Triplicates were done and the ratio of the MFI (UCHT1) versus MFI (Jovi1) is displayed. Since this ratio was similar, we conclude that the TMchim TCR was folded properly concerning the two epitopes bound by these antibodies.

(G) Binding of the wt and TMchim TCR to cholesterol- (left) or palmitate (right) -coupled beads was quantified and calculated as in Figure 1F, showing that the capacity to bind to cholesterol, but not to palmitate, was reduced in the TMchim TCR compared to the wt TCR.

(H) Cells were stimulated as in Figure 2B with the exception that the stimulation lasted for 7 h. Then cells were stained with an APC-coupled anti-CD69 antibody and analysed by flow cytometry. The percent of CD69-positive living cells is displayed. This experiment shows that the mutant TCR defective in cholesterol binding is partially active in non-stimulated cells.

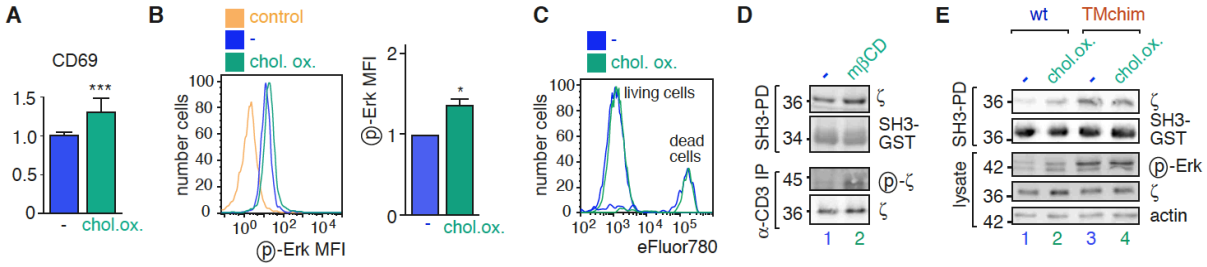

Figure S3. Cholesterol prevents spontaneous TCR signaling, Related to Figure 3

(A) Jurkat cells were treated with cholesterol oxidase or not for 6 hours. The cells were then stained with anti-CD69 antibodies and analysed by flow cytometry. The normalized MFI is shown.

(B) Human peripheral blood mononuclear cells (PBMCs) from a healthy donor were left untreated (-) or treated with cholesterol oxidase for 1 h at 37°C. Cells were fixed, permeabilized, stained with anti-phospho-Erk and anti-CD3ε (UCHT1). The mean fluorescence intensity (MFI) of phospho-Erk on gated UCHT1-positive cells is shown (left panel). As a negative control, untreated T cells were stained solely with the secondary antibody (yellow histogram). The normalised MFI of phospho-Erk on gated UCHT1-positive cells is shown in the right panel. As observed in Jurkat cells (Figure 3B), cholesterol oxidation in PBMCs also led to a statistically significant increase in phospho-Erk.

(C) Jurkat cells were treated with cholesterol oxidase for 1 h at 37°C or not. Subsequently, cells were stained with the Fixable Viability Dye eFluor 780 (eFluor780, eBioscience) and measured by flow cytometry. Living and dead cells, which spontaneously occur in small amounts in our cultures, were gated using the forward and side scatter. The intensity of the fluorescent dye in each gate displayed. This experiment shows that cholesterol oxidase did not affect viability of the cells.

(D) Jurkat cells were treated with 10 mM methyl-β-cyclodextrin for 1 min at 37°C or left untreated. The SH3-PD assay to measure active TCRs, and anti-CD3ε IP were performed as above. This experiment shows that cholesterol extraction leads to a switch of the TCRs from TCR_I to TCR_A and to weak phosphorylation of CD3ζ.

(E) wt scTCRβ- and TMchim scTCRβ-expressing cells were left untreated or treated with cholesterol oxidase for 1 hr. After lysis, an SH3-PD assay was carried out. The purified proteins and the lysate were subjected to WB analysis as shown. This experiment indicates that in the TMchim TCRs defective in cholesterol binding the equilibrium between TCR_I and TCR_A is shifted towards the active state, and that cholesterol oxidation does not further cause that the TMchim TCRs switch to the active conformation. Likewise, phospho-Erk levels are not increased by cholesterol oxidation in the TMchim TCR-expressing cells.

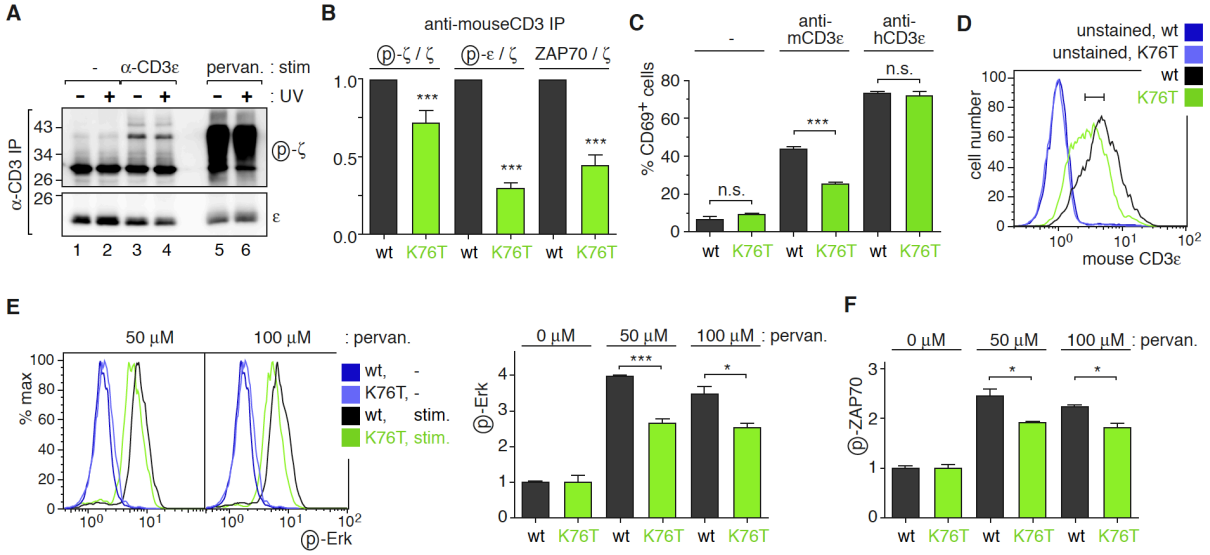

Figure S4. The K76T CD3ε-containing TCR has impaired signaling activity, Related to Figure 4

(A) Jurkat cells were illuminated with UV light or not. Subsequently, the cells were left unstimulated, or stimulated for 5 min at 37°C with anti-human CD3ε (OKT3) or pervanadate. After cell lysis an anti-CD3 immuno-precipitation was performed, proteins separated by SDS-PAGE and visualised in WB using anti-phosphoY142-CD3ζ and anti-CD3ε antibodies. This experiment demonstrates that UV exposure prior to anti-CD3 or pervanadate treatment did neither influence the background nor the stimulus-induced phosphorylation of CD3ζ.

(B) The background-corrected band intensities of phospho-CD3ζ, phospho-CD3ε and TCR-recruited ZAP70 were divided by the band intensities of CD3ζ as shown in figure 4E, lanes 3-6. Values of the wt murine TCR were normalized to 1. Phosphorylation of CD3 and ZAP70, as well as its recruitment to the mutant K76T TCR were statistically reduced.

(C) Jurkat cells expressing wt and K76T murine CD3ε were left unstimulated (-), stimulated with 12μg/ml anti-mouse CD3ε (145-2C11) or anti-human CD3ε (OKT3). After incubation for 6 h at 37°C, cells were analysed for CD69 expression by flow cytometry. The percent of CD69-positive living cells is displayed. The results show that the K76T TCR has a statistically significantly reduced capacity to upregulate CD69 expression upon anti-mouse CD3 stimulation. As a control, the endogenous wt TCRs stimulated with anti-human CD3, were functional in both cells.

(D) The cells as in (C) were stained with the anti-mouse CD3ε antibody 145-2C11 (black and green), or left unstained (light and dark blue). The region gated for equal expression of the TCR is indicated.

(E) The cells as in (C) were left untreated or stimulated for 5 min with pervanadate as indicated. After fixation cells were stained with anti-mouse CD3ε and after further permeabilisation with anti-phospho-Erk antibodies. After flow cytometric measurement, cells were gated on similar TCR expression (the gate is shown in (D) and the fluorescence intensity of phospho-Erk plotted (left panel). The MFI of the phospho-Erk signals were normalized to the unstimulated wt or K76T cells (right panel).

(F) Cells were stimulated stained and analysed as in (E) with the exception that anti-phospho-ZAP70 was used instead of anti-phospho-Erk. The MFI of the phospho-ZAP70 signals were normalized to the unstimulated wt or K76T cells.

Together, these experiments show that the mutant K76T TCR, which cannot switch to the TCR_A, state has an impaired signalling capacity whether stimulated by antibodies (as published (Martinez-Martin et al., 2009)) or pervanadate, which inhibits phosphatases but does not change the TCR_I-TCR_A equilibrium (Gil et al., 2002).

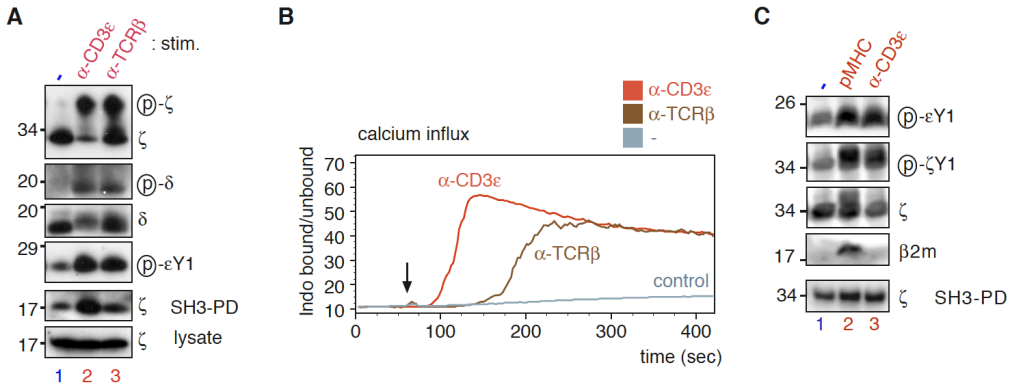

Figure S5. Only TCRs in the active state are accessible for phosphorylation, Related to Figure 5

(A) The lysates of wt scTCRβ-expressing cells were left untreated or incubated with the indicated antibodies for 90 minutes at 4ºC. TCRs were then purified with nitro-phenol-coupled beads and incubated with recombinant, active Lck and ATP at 30°C for 30 minutes. The reaction was stopped by adding non-reducing sample buffer. The purified TCRs were further treated with N-glycosidase F to cleave N-linked carbohydrate moieties and allow us to distinguish electrophoretically between the CD3ε and CD3δ chains. In parallel, the SH3-PD assay was performed and an aliquot of the total cellular lysate was loaded as a control. WB was done using anti-ζ, anti-phospho-tyrosine (4G10), anti-δ, anti-phospho-εY1, anti-ζ and anti-ζ antibodies (top to bottom).

(B) wt scTCRβ-expressing cells were loaded with Indo-1 and stimulated with the indicated antibodies to induce TCR-mediated Ca^{2+} responses. PBS was added to the control. The Indo-1 ratio was integrated over 8 minutes and measured by flow cytometry. The stimuli were added after 1 minute. Together with A) this experiment shows that the amount of TCRs in the TCR_A state correlates with the amount of Ca^{2+} influx.

(C) Membrane patches of T1.4 cells were treated with pMHC tetramers, anti-CD3ε (145-2C11) antibodies or left untreated and then irradiated with UV-light to crosslink the pMHC tetramers to the TCRs. After addition of ATP and recombinant-active Lck, phosphorylation reactions were carried out for 15 min at 30°C. Proteins were then analysed by WB using anti-phospho-εY1, anti-phospho-tyrosines (4G10), anti-ζ and anti-β2 microglobulin antibodies (top to bottom). In parallel, the SH3-PD assay was performed (lower panel).

This figure shows that stabilisation of the TCR_A state by pMHC tetramer or antibody stimulation renders the ITAMs of CD3ε, CD3δ and CD3ζ available for phosphorylation by active Lck.

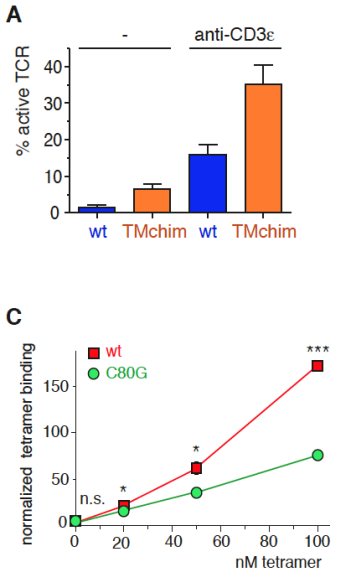

B

parameter	formula	value	comment
L, conformational equilibrium constant in absence of cholesterol or pMHC binding	$L = [TCR_I] / [TCR_A]$	14 [12,16]	
K_a, equilibrium constant for monovalent pMHC binding to TCR_A and TCR_I	$K_a = [TCR_A\text{-pMHC}] / ([TCR_A]x[pMHC])$ = $[TCR_I\text{-pMHC}] / ([TCR_I]x[pMHC])$	0.1 [0.07,1.13] μM^{-1}	depends on the pMHC-TCR pair
K_b, equilibrium constant for bivalent pMHC binding to TCR_A	$K_b = [TCR_A{=}pMHC] / [TCR_A\text{-pMHC}]$	1755 [1417,2650]	
K_c, equilibrium constant for cholesterol binding to TCR_I	$K_c = [TCR_I\text{-cholesterol}] / ([TCR_I] \times [\text{cholesterol}])$	6×10^5 m^2/mol	assuming a membrane concentration of 1 molecule cholesterol / nm^2
K_r, equilibrium ratio of cholesterol-bound to unbound TCRs	$K_r = [TCR_I\text{-cholesterol}] / [TCR_I]$	1	

Figure S6. A lipid-regulated allosteric model for TCR triggering, Related to Figure 6

A) Wt and TMchim TCR-expressing cells were left unstimulated (-) or stimulated with 5 µg/ml anti-CD3ε (OKT3) for 5 min at 37°C. After lysis the lysate was split in two halves, an SH3-PD (TCR_As) and an anti-CD3ε immuno-precipitation (total TCRs) were performed. Purified proteins were analysed by WB using anti-CD3ζ antibodies. The percentage of active TCRs was calculated from the CD3ζ band intensities (n=3).

B) Calculation of the parameters and their values according to the allostery model of TCR phosphorylation in Figure 6A. In the third column the 95% confidence intervals are given in brackets.

C) Lymph node cells as in Figure 6C were stained on ice for 30 min with increasing concentrations of PE-labeled wt OVA-H2-K^b tetramers (that can bind to CD8) and then with an anti-Vα2 antibody. Flow cytometry measurement to quantify the amount of bound tetramers was done as in Figure 6C (n=3), including gating on cells with similar TCR expression level and normalization to the TCR level. * $p < 0.05$, *** $p < 0.001$ by unpaired t-test.

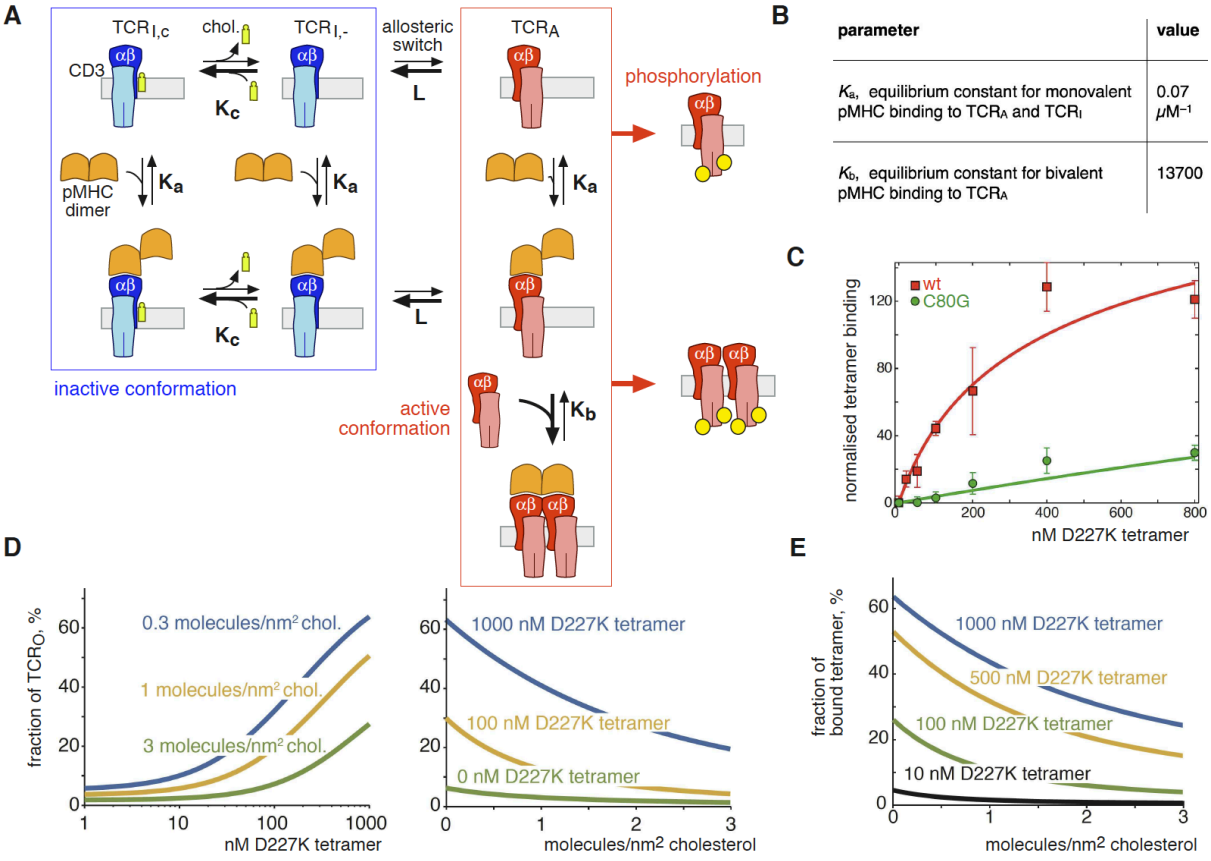

Figure S7. Allosteric model for TCR triggering with ligand-induced TCR clustering, Related to Figure 6

(A) This model is analogue to the one from Figure 6, except that TCRs are expressed as monomers and only cluster upon multivalent pMHC binding (crosslinking). In this model pMHC dimers can only cluster two TCR_A, but not two TCR_I or TCR_A with TCR_I. The partition function of this model is given by $Z = 1 + \alpha + \alpha\beta[T] + L(1+\alpha)(1+\gamma)$ where $[T]$ denotes the concentration of pMHC-unbound TCR_A and all other parameters are as defined in Supplemental Experimental Procedures.

(B) All calculated parameters of the "ligand-induced TCR clustering" model from (A) were the same as in the related model from Figure 6A, except K_a and K_b, which are shown here.

(C) The experimental D227K-pMHC tetramer binding data from Figure 6C were used to fit to the "ligand-induced TCR clustering" model from panel A. The best fit of the model to the data is shown by solid lines, indicating that this model is also in line with the data. Thus, the clustering mechanism of the TCR does not affect the interpretation of the data.

(D, E) Analyses of the "ligand-induced TCR clustering" model were done as in Figures 6D and 6E. The results are very similar, indicating that the role of cholesterol in controlling the conformational switch in the TCR and in regulating pMHC tetramer binding is independent of whether TCR are nanoclustered or clustered by the pMHC tetramer.

SUPPLEMENTAL EXPERIMENTAL PROCEDURES

Cells, Cloning and Transfection

The mouse T-cell line T1.4, the human T-cell line Jurkat, variants of Jurkat, the human B-cell line J558Lmb1/δm and the mouse T-cell lines M.mζ-SBP and M.hTfR-SBP (Molnar et al., 2012) were grown in complete RPMI-1640 medium supplemented with 5% bovine serum and antibiotics at 37°C. Human peripheral blood mononuclear cells were isolated from healthy donors according to the local ethics committee requirements for human experimentation and purified by Ficoll gradient centrifugation. Jurkat cells were transduced with lentiviruses harbouring the plasmids pHRSIN-mCD3ε and pHRSIN-mCD3ε(K76T) (Martinez-Martin et al., 2009) to yield J.mCD3ε and J.mCD3ε(K76T). pHRSIN-mCD3ε(C80G) was also used, but in this case the Jurkat transductants did not express large amounts of the mutant TCR on their surface (data not shown).

To generate the wt scTCR and the TMchim scTCR, the following strategy was used. The coding sequence for the scTCRβ chain was amplified by PCR from pSRscTCRβ (Minguet et al., 2007) and cloned into the HpaI/EcoRI site of pCDNA3.1 to yield the retroviral expression vector pCDNA3-scTCRβ. The expression vector pCDNA3-scTCRβ-γTM was generated by linking the PCR product corresponding to the leader peptide and extracellular regions of the scTCRβ molecule to the PCR product corresponding to the TM and cytoplasmic domains of the human TCRγ2 molecule by nested PCR and cloning the resulting PCR product into the HpaI/EcoRI site of pCDNA3.1 The Jurkat-derived TCRβ-negative cell line 31-13 was transfected with the plasmids pCDNA3-scTCRβ or pCDNA3-scTCRβ-γTM to yield 31-13.scTCRβ (wt scTCRβ) and 31-13.scTCRβ-γTM (TMchim scTCRβ) cell lines.

Reagents

The following antibodies were used: anti-CD3ε and anti-CD3δ (M20ε and M20δ, Santa Cruz Biotechnology), anti-hCD3-Alexa647 (UCHT1 Biolegend), anti-phospho-tyrosine (4G10, Upstate Biotechnology), anti-ζ 448 (San Jose et al., 1998), anti-phospho-Erk (Cell Signalling), anti-Erk2 (BD Transduction), anti-hCD3 (UCHT1, Dr. Beverly, UK), anti-hCD3ε (OKT3, Ortho), anti-mCD3ε (145-2C11, Biolegend), anti-mCD3ε APC (145-2C11, eBioscience), anti-CD69 FITC (Biolegend), anti-Bub3 (Abcam), anti-TfR (7F8, Abcam), anti-IgD-HRPO (Nordic), anti-TCR Cβ1 (Jovi1), anti-Vα2 PE (B20.1, BD Pharmingen), anti-phospho-εY1 (Dopfer et al., 2010), pan anti-phospho-ζ (also called anti-phospho-εY2) (Dopfer et al., 2010), anti-phospho-ζ (pY142, Sigma) anti-β2microglobulin (Santa Cruz Biotechnology), anti-phospho ZAP70 (phospho-319, BD Biosciences or Cell Signalling), anti-ZAP70 (Santa Cruz Biotechnology), anti-actin (Sigma), anti-rabbit DyLight633 (Thermo Scientific), anti-mouse IgG PE (Southern Biotech), anti-mouse IgG APC (Southern Biotech), anti-GST (Bethyl) and secondary antibodies for Western Blot (Southern Biotech, LI-COR). Nitro-iodo-phenol and nitro-phenol-coupled beads were purchased from Biosearch Technologies. N-glycosidase F was from Roche Diagnostics, cholesterol oxidase, MβCD and all other chemicals were from Sigma. Recombinant active GST-Lck was from Enzo Life Sciences. Since GST is at the N-terminus and the fusion protein expressed in *E. coli*, GST-Lck neither contains N-myristoylations (Duronio et al., 1990; Knoll and Gordon, 1993) nor S-palmitoylations (Greentree and Linder, 2004), and thus is not post-translationally modified by any fally acid.

Ca^{2+} influx

Cells resuspended in RPMI-1640 medium with 1% serum were incubated with 5 μg/ml Indo-1 and 0.5 μg/ml of pluronic F-127 (both Molecular Probes) at 37°C for 45 minutes. After washing, cells were resuspended in RPMI-1640 medium with 1% serum and kept on ice. Ca^{2+} influx was induced by addition of the indicated stimuli 1 min after starting to record the ratio of Ca^{2+}-bound Indo-1 versus unbound Indo-1 with a LSRII fluorescence spectrometer (Becton Dickinson). Data were analysed with FlowJo 8.2 software.

Cell treatments and lysis

5 - 30 million cells were harvested per sample, resuspended in 0.5 - 1 ml medium without serum, and incubated for 1 h at 37°C. TCR stimulation was performed at 37°C with 5 μg/ml antibody (anti-mCD3ε clone 145-2C11, anti-hCD3ε clone UCHT1 or clone OKT3 as indicated and anti-TCRβ clone Jovi1) or the given concentrations of pervanadate (50 μM: 100 μl Na_3VO_4 50 mM, 0.5 μl H_2O_2) for 5 minutes, if not otherwise indicated. To oxidize cell surface cholesterol, 30 million cells were pelleted per sample, resuspended in 1 ml RPMI-1640 medium supplemented with 5% lipid-depleted, charcoal-stripped fetal calf serum (Biowest), and incubated for 1 hour at 37°C. Subsequently, cells were treated with 0.5 U/ml cholesterol oxidase (Sigma) at 37ºC for the times indicated. To extract cholesterol, cells were treated with 10 mM methyl-β-cyclodextrin at 37°C for the times indicated. Dead cell were stained with a 1:1000 dilution of the Fixable Viability Dye eFluor® 780 (eBiosciene) 30 min before the flow cytometric measurement.

Cell lysis was done in 1 ml lysis buffer containing 20 mM TrisHCl (pH8), 137 mM NaCl, 2 mM EDTA, 10% glycerol, protease inhibitor cocktail (Sigma), 1 mM PMSF, 5 mM iodoacetamide, 0.5 mM sodium orthovanadate, 1 mM NaF and 0.05% - 0.5% Brij96 for 15 minutes on ice, followed by a 15 minutes centrifugation in an Eppendorf centrifuge to pellet the nuclei and insoluble materials.

Reconstitution of CD3 phosphorylation in membranes

Membrane fractions were prepared by disrupting 3 x 10^7 T1.4, Jurkat or 31-13.scTCRβ cells in hypoosmotic buffer (10 mM HEPES [pH 7.4], 42 mM KCl, 5 mM MgCl2, and protease inhibitors) with a Dounce homogenizer and pelleting the membranes in an ultracentrifuge at 150,000 x g. The membranes from T1.4 cells were resuspended in PBS supplemented with 50 mM pMHC tetramer (4P peptide: (SYIPSAEK(ABA)I, H2Kd, kindly provided by Immanuel Lüscher (Luescher et al., 1994)) or 20 μg/ml anti-CD3 (145-2C11). After addition of active-recombinant GST-Lck and ATP, CD3 phosphorylation was done as above.

Allostery model of TCR opening

The model considers a preformed TCR dimer bound by dimeric pMHC ligands. Following the Monod-Wyman-Changeux model (Monod et al., 1965), we assume that the two TCRs can undergo a concerted transition between the inactive (TCR_ITCR_I) and the active (TCR_ATCR_A) conformations; the conformational equilibrium constant in the absence of pMHC or cholesterol is denoted by $L = [TCR_ITCR_I]/[TCR_ATCR_A]$, for simplicity expressed as $L = [TCR_I]/[TCR_A]$. Both TCR_I and TCR_A bind pMHC monovalently with the same affinity K_a (in addition to the states shown in Figure 6A, a TCR dimer can also bind to pMHC monovalently). In the active conformation, a single monovalently bound ligand can bind the second TCR with affinity K_b. In the inactive state, cholesterol binds to the TCR with equilibrium constant K_c. Defining the dimensionless parameters $\alpha = K_a$ x [pMHC], $\beta = K_b$,

and $\gamma = K_c$ x [cholesterol], where [pMHC] and [cholesterol] denote the concentrations of free pMHC dimers and membrane cholesterol, respectively, the partition function of this system reads: $Z = (1+\alpha)^2 + \alpha\beta + L[(1+\alpha)^2 + (1+\gamma)^2]$. From Z, the fractions of the various states shown in Figure 6 were calculated. For all experiments with unstimulated cells, $\alpha = 0$. To simulate the anti-CD3 activation experiments (Figure 6B), we used the wt TCR data to fit the effective free parameters α and $\beta / (1+ \alpha)^2$, thus fixing the degree of crosslinking by anti-CD3, and used these parameters to make the prediction for TMchim TCR. For fitting the pMHC binding data in Figure 6C, we used the L and K_c determined above and estimated K_a and K_b by a maximum likelihood approach; for the C80G CD3ε mutant, $L \rightarrow \infty$. 95% confidence intervals were calculated by parametric bootstrap. For Figure 6D, we took $K_a = 1\ \mu M^{-1}$ to compute α for the given pMHC concentrations (Huang et al., 2010).

Additionally we developed a model without pre-clustering of the TCR (Figure S7). Here, the partition function is given by $Z = 1 + \alpha + \alpha\beta[T] + L(1+ \alpha)(1+\gamma)$ where [T] denotes the concentration of open TCRs that did not bind to ligand. The remaining notation is as given above.

SUPPLEMENTAL REFERENCES

Arnett, K.L., Harrison, S.C., and Wiley, D.C. (2004). Crystal structure of a human CD3-ε/δ dimer in complex with a UCHT1 single-chain antibody fragment. Proc. Natl. Acad. Sci. USA *101*, 16268-16273.

Backstrom, B.T., Milia, E., Peter, A., Jaureguiberry, B., Baldari, C.T., and Palmer, E. (1996). A motif within the T cell receptor α chain constant region connecting peptide domain controls antigen responsiveness. Immunity *5*, 437-447.

Dopfer, E.P., Schopf, B., Louis-Dit-Sully, C., Dengler, E., Hohne, K., Klescova, A., Prouza, M., Suchanek, M., Reth, M., and Schamel, W.W. (2010). Analysis of novel phospho-ITAM specific antibodies in a S2 reconstitution system for TCR-CD3 signalling. Immunol. Lett. *130*, 43-50.

Duronio, R.J., Jackson-Machelski, E., Heuckeroth, R.O., Olins, P.O., Devine, C.S., Yonemoto, W., Slice, L.W., Taylor, S.S., and Gordon, J.I. (1990). Protein N-myristoylation in Escherichia coli: reconstitution of a eukaryotic protein modification in bacteria. Proc. Natl. Acad. Sci. USA *87*, 1506-1510.

Gil, D., Schamel, W.W., Montoya, M., Sanchez-Madrid, F., and Alarcon, B. (2002). Recruitment of Nck by CD3 epsilon reveals a ligand-induced conformational change essential for T cell receptor signaling and synapse formation. Cell *109*, 901-912.

Greentree, W.K., and Linder, M.E. (2004). Purification of recombinant G protein α subunits from Escherichia coli. Meth. Mol. Biol. *237*, 3-20.

Huang, J., Zarnitsyna, V.I., Liu, B., Edwards, L.J., Jiang, N., Evavold, B.D., and Zhu, C. (2010). The kinetics of two-dimensional TCR and pMHC interactions determine T-cell responsiveness. Nature *464*, 932-936.

Huppa, J.B., and Ploegh, H.L. (1997). In vitro translation and assembly of a complete T cell receptor-CD3 complex. J. Exp. Med. *186*, 393-403.

Knoll, L.J., and Gordon, J.I. (1993). Use of Escherichia coli strains containing fad mutations plus a triple plasmid expression system to study the import of myristate, its activation by Saccharomyces cerevisiae acyl-CoA synthetase, and its utilization by S. cerevisiae myristoyl-CoA:protein N-myristoyltransferase. J. Biol. Chem. *268*, 4281-4290.

Luescher, I.F., Cerottini, J.C., and Romero, P. (1994). Photoaffinity labeling of the T cell receptor on cloned cytotoxic T lymphocytes by covalent photoreactive ligand. J. Biol. Chem. *269*, 5574-5582.

Martinez-Martin, N., Risueno, R.M., Morreale, A., Zaldivar, I., Fernandez-Arenas, E., Herranz, F., Ortiz, A.R., and Alarcon, B. (2009). Cooperativity between T cell receptor complexes revealed by conformational mutants of CD3ε. Sci. Signal. *2*, ra43.

Minguet, S., Swamy, M., Alarcon, B., Luescher, I.F., and Schamel, W.W. (2007). Full activation of the T cell receptor requires both clustering and conformational changes at CD3. Immunity *26*, 43-54.

Molnar, E., Swamy, M., Holzer, M., Beck-Garcia, K., Worch, R., Thiele, C., Guigas, G., Boye, K., Luescher, I.F., Schwille, P., *et al*. (2012). Cholesterol and sphingomyelin drive ligand-independent T-cell antigen receptor nanoclustering. J. Biol. Chem. *287*, 42664-42674.

Monod, J., Wyman, J., and Changeux, J.P. (1965). On the nature of allosteric transitions: a plausible model. J. Mol. Biol. *12*, 88-118.

Petersen, T.R., Gulland, S., Bettelli, E., Kuchroo, V., Palmer, E., and Backstrom, B.T. (2004). A chimeric T cell receptor with super-signaling properties. Int. Immunol. *16*, 889-894.

San Jose, E., Sahuquillo, A.G., Bragado, R., and Alarcon, B. (1998). Assembly of the TCR/CD3 complex: CD3 epsilon/delta and CD3 epsilon/gamma dimers associate indistinctly with both TCRα and TCRβ chains. Evidence for a double TCR heterodimer model. Eur. J. Immunol. *28*, 12-21.